https://doi.org/10.5194/nhess-2019-178
Preprint. Discussion started: 11 June 2019

Natural Hazards and Earth System Sciences
Discussions

Geologic and geomorphic controls on rockfall hazard: how well do past rockfalls predict future distributions?

Josh Borella [1,2] , Mark Quigley [3,2], Zoe Krauss [4,1], Krystina Lincoln [5,1], Januka Attanayake [3], Laura Stamp [5,1], Henry Lanman [6,1], Stephanie Levine [7,1], Sam Hampton [1,2], Darren Gravley [1,2]

[1] Frontiers Abroad, 3 Harbour View Terrace, Christchurch, 8082, New Zealand
[2] Department of Geological Sciences, University of Canterbury, Christchurch, 8041, New Zealand
[3] School of Earth Sciences, The University of Melbourne, Victoria, 3010, Australia
[4] Department of Geology, Colorado College, Colorado Springs, CO, 80903, USA
[5] Department of Geosciences, Williams College, Williamstown, MA, 01267, USA
[6] Department of Geology, Whitman College, Walla Walla, WA, 99362, USA
[7] Department of Geology, Carleton College, Northfield, MN, 55057, USA

Correspondence: Josh Borella (josh@frontiersabroad.com)

KEYWORDS: Rockfall hazard, boulder spatial distributions, frequency-volume distributions, Canterbury Earthquake Sequence, prehistoric rockfall boulders, deforestation, rockfall source characteristics, rockfall physical properties, rockfall numerical modelling, rockfall, Christchurch

Abstract

To evaluate the geospatial hazard relationships between recent (contemporary) rockfalls and their prehistoric predecessors, we compare the locations, physical characteristics, and lithologies of rockfall boulders deposited during the 2010-2011 Canterbury earthquake sequence (CES) (n=185) with those deposited prior to the CES (n=1093). Population ratios of pre-CES to CES boulders at two study sites vary spatially from 5:1 to 8.5:1. This is interpreted to reflect *(i)* variations in CES rockfall flux due to intra- and inter-event spatial differences in ground motions (e.g., directionality) and associated variations in source cliff responses, *(ii)* possible variations in the triggering mechanism(s), frequency, flux, record duration, boulder size distributions, and post-depositional mobilization of pre-CES rockfalls relative to CES rockfalls, and *(iii)* geological variations in the source cliffs of CES and pre-CES rockfalls. On interfluves, CES boulders traveled approximately 100 to 350 m further downslope than prehistoric (pre-CES) boulders, interpreted to reflect reduced resistance to CES rockfall transport due to preceding anthropogenic hillslope de-vegetation. Volcanic breccia boulders are more dimensionally equant, rounded, larger, and traveled further downslope than coherent lava boulders, illustrating clear geological control on rockfall hazard. In valley bottoms, the furthest-traveled pre-CES boulders are situated further downslope than CES boulders due to *(i)* remobilization of pre-CES boulders by post-depositional processes such as debris flows, and *(ii)* reduction of CES boulder velocities and travel distances by collisional impacts with pre-CES boulders. A considered earth-systems approach is required when using preserved distributions of rockfall deposits to predict the severity and extents of future rockfall events.

https://doi.org/10.5194/nhess-2019-178
Preprint. Discussion started: 11 June 2019

Natural Hazards and Earth System Sciences
Discussions

1 Introduction

Rockfall deposits pervade many mountainous and hilly regions worldwide (Varnes, 1978; Evans and Hungr, 1993; Wieczorek, 2002; Dorren, 2003; Guzzetti et al., 2003) and can provide important data for assessing future rockfall hazards (Porter and Orombelli, 1981; Keefer, 1984; Dussauge-Peisser et al., 2002; Copons and Vilaplana, 2008; Wieczorek et al., 2008; Stock et al., 2014; Borella et al., 2016a). Their characteristics (e.g. location, size, morphology) may be used to complement numerical rockfall modeling scenarios (Agliardi and Crosta, 2003; Dorren et al., 2004; Heron et al., 2014; Vick, 2015; Borella et al., 2016a) and inform engineering-design criteria for rockfall mitigation structures (e.g. impact fences, tiebacks, protection forests) (e.g. Agliardi and Crosta, 2003; Dorren et al., 2004; Guzzetti et al., 2004). However, natural and anthropogenic changes to the landscape (including changes to the rockfall source and slope areas) between successive rockfall events and the post-depositional history for rockfalls can be complex (e.g. Borella et al., 2016a,b). To better understand how past rockfalls provide suitable proxies for characterizing future hazard, comparisons between the geologic and geomorphic attributes of individual rockfall events and cumulative amalgamations of many events are valued. Critical evaluations of possible intervening changes to the landscape that may influence the mechanics of rockfall production and travel are an important component of these studies.

More than 7000 mapped individual rocks fell from cliffs in the Port Hills in southern Christchurch during the 2010-2011 Canterbury Earthquake Sequence (CES) in New Zealand's South Island (Massey et al., 2014). Most of the rockfalls (>6000) occurred during the 22 February 2011 moment magnitude (Mw) 6.2 and 13 June 2011 Mw 6.0 Christchurch earthquakes (Massey et al., 2014). Approximately 200 houses were impacted, 100 houses severely damaged, and five fatalities caused by falling rocks in the 2011 February earthquake (Massey et al., 2014; Grant et al., 2018). CES rockfalls were characterized by boulder-size distribution, runout distance (the distance a rock travels down a slope from its source), source-area dimensions, and boulder-production rates over a range of triggering peak ground accelerations (Massey et al., 2012a-e, 2014, 2017; Quigley and Mackey, 2014; Quigley et al., 2016).

Subsequent field investigations revealed an abundance of pre-CES rockfall deposits in CES rockfall areas (Townsend and Rosser, 2012; Mackey and Quigley, 2014; Borella et al.,

https://doi.org/10.5194/nhess-2019-178
Preprint. Discussion started: 11 June 2019


Natural Hazards and Earth System Sciences
Discussions

2016a,b), suggesting multiple rockfall events had occurred at these sites in the past (Mackey and Quigley, 2014; Borella et al., 2016a,b; Sohbati et al., 2016). Retrospectively, these pre-CES deposits had potential value to have contributed to hazard assessments during land-planning and urban development in Christchurch prior to the CES; however, there is no evidence that they did so (Townsend and Rosser, 2012; Litchfield et al., 2016). At one well-studied location (Rapaki) in the Port Hills of southern Christchurch, CES and pre-CES boulder populations were shown to have similar volumetric size and morphology characteristics, but a significant population of CES boulders had longer maximum runout distances than their pre-CES counterparts (Borella et al., 2016a). Pre-CES rockfalls were dated using independent approaches to >3-15 ka (Mackey and Quigley, 2014; Sohbati et al., 2016; Borella et al., 2016b). With the aid of numerical modeling of rockfall trajectories (using RAMMS - rapid mass movement simulation), these data were collectively interpreted to suggest that anthropogenic deforestation between pre-CES and CES rockfalls was the primary cause for the observed spatial distinctions in CES and pre-CES rockfall distributions (Borella et al., 2016a). Elsewhere in the Port Hills and greater Banks Peninsula, the causes for differences in the spatial distribution between CES and pre-CES rockfalls are less clear and in some locations the current positions of pre-CES boulders extend further distances from source cliffs than their CES counterparts. A more integrated and regional understanding of the geologic and geomorphic controls on rockfall distributions has the potential to inform rockfall hazard analyses for land-zoning and engineering considerations here and elsewhere (e.g. Lan et al., 2010).

In this study we document the location, volume, morphology, and lithology for individual (n=1093) pre-CES rockfall boulders at two sites (Rapaki and Purau) in the Banks Peninsula near Christchurch, New Zealand. The spatial distributions and physical attributes for pre-CES boulders are compared to rockfall boulders (n=185) deposited at the same sites during the 2010-2011 CES. RAMMS bare-earth and forested numerical modelling scenarios are conducted to help evaluate the influence of geologic, geomorphic, and anthropogenic factors on rockfall distributions, identify boulder sub-populations that have likely experienced post-emplacement mobility, determine the relative timing of pre-existing rockfalls (i.e. prehistoric or historic), and evaluate the efficacy of RAMMS in replicating empirical CES and prehistoric boulder spatial distributions. We highlight the complexity of interpreting future rockfall hazard based on former boulder distributions (particularly location) due to: (i) potential landscape changes including deforestation, (ii) changes in rockfall source (e.g. progressive emergence of bedrock sources from beneath sedimentary cover), (iii) remobilization of prior rockfalls by surface

https://doi.org/10.5194/nhess-2019-178
Preprint. Discussion started: 11 June 2019


Natural Hazards and Earth System Sciences
Discussions

processes including debris flows (primarily in channels), (iv) lithological variability effects on the type of material liberated in successive events, (v) collisional impedance with pre-existing boulders (particularly in channels/valleys), and (vi) variations in the location, size, and strong ground motion characteristics of past rockfall-triggering earthquakes and their impact on rockfall flux and boulder mobility.

2 Geologic Setting

2.1 Overview

Banks Peninsula, located on the east coast of New Zealand's South Island, is comprised of three main volcanoes (Lyttelton, Akaroa, and Mt. Herbert) active between 11.0 and 5.8 Ma (Hampton and Cole, 2009) (Fig. 1). The two study sites (Rapaki and Purau) are located within the inner crater rim of the Lyttelton Volcanic complex (Figs. 1, 2, 3), the oldest of the volcanic centers and thought to be active from 11.0 to 9.7 Ma (Hampton and Cole, 2009). Source rock at both sites is classified by Sewell (1988) and Sewell et al. (1992) as part of the Lyttelton Volcanic Group (LVG) and consists of basaltic to trachytic lava flows interbedded with breccia and tuff (Mvl). Numerous dikes and minor domes are observed within the LVG. Our field observations support the reported lithologic descriptions for the two study locales. The inferred strike and dip for lava flows nearest to the study sites indicates a shallow inclination in a predominantly northerly direction for measurements nearest the Rapaki and Purau study sites (Hampton and Cole, 2009). Sewell et al. (1992) reports a similar shallow northerly to northwesterly dip of 12° for lava flows nearest Rapaki. The study areas were selected because both have abundant pre-CES and CES rockfall boulders (Fig. 4) derived from lithologically equivalent volcanic source rocks. Rapaki represents a case study location proximal to the source of the 2011 February and June Christchurch earthquakes (epicenters ~2.5-5.0 km; hypocenters ~ 5.6-7.0 km), while Purau is located more distally (epicenters ~6.6-8.4 km; hypocenters ~8.9-10.3 km). Estimated rockfall-generating peak horizontal ground velocities (PGV) at the Rapaki site in the February and June earthquakes were ≥ 30 cm s^{-2} (Mackey and Quigley, 2014).

2.2 Rapaki study site

https://doi.org/10.5194/nhess-2019-178
Preprint. Discussion started: 11 June 2019


Natural Hazards and Earth System Sciences
Discussions

149 The Rapaki study site is situated in the Port Hills of southern Christchurch (Figs. 1, 2) on the
150 southeastern slope of Mount Rapaki (*Te Poho o Tamatea*), which has a summit height of ~400
151 meters. The study hillslope is slightly concave to planar with a total area of ~0.21 km^2 and
152 faces to the east-southeast. The source zone consists of steep to subvertical bedrock cliffs
153 composed of stratified basaltic lava and indurated auto-breccia or pyroclastic flow deposits
154 (Fig. 5A-C). Breccia layers are thicker (~3-10 meters) and jointing is more widely spaced
155 (often >10 m). Coherent lava layers are comparably thin (<3 meters) and joints are more closely
156 spaced (generally <1-2 meter). Total height and length of the source rock are ~60 meters and
157 ~300 meters, respectively (Fig. 5A). Below the source area, is a ~23°, grassy hillslope
158 composed of windblown sediment deposits (loess), loess and volcanic colluvium, and
159 overlying rockfall boulders (both CES and pre-CES) (Bell and Trangmar, 1987). Rapaki village
160 (estimated population=100 residents) lies at the hillslope base at elevations of ~70 meters (asl)
161 to sea level (Figs. 3, 4). Anthropogenic deforestation has exposed a hillslope that is currently
162 experiencing accelerated erosion (Borella et al., 2016a,b) in the form of mass wasting and
163 tunnel gully formation. Shallow landslides, including debris and earth flows, are most prevalent
164 in upper to mid-slope positions, while rill and gulley erosion predominate in lower slope
165 positions.
166
167 Rockfall is a dominant surface feature at the Rapaki study site (Mackey and Quigley, 2014;
168 Vick, 2015; Borella et al., 2016a,b). Pre-CES and CES rockfall boulders at the study site can
169 be divided into two dominant lithology types: volcanic breccia (VB) and coherent lava (CL)
170 basalt. During the 22 February and 13 June 2011 earthquakes, more than 650 individual CES
171 boulders ranging in diameter from <15 cm to >3m were dislodged from the volcanic source
172 rock near the top of Mount Rapaki, many impacting and destroying residential homes (Massey
173 et al., 2014; Mackey and Quigley, 2014).
174
175 **2.3 Purau study site**
176
177 Purau is located on the southern side of Lyttelton Harbour, approximately 5 kilometers
178 southeast of Rapaki (Figs. 1, 3). Slopes at Purau have a west-northwest aspect, the opposite of
179 the Rapaki study hillslope. Mapping of pre-CES and CES rockfall was performed on and within
180 several interfluves (spurs) and bounding valleys, respectively (Fig. 3) and encompassed a total
181 area of ~1.4 km^2. The source rock geology at Purau, including lithology and structure, is
182 equivalent to that observed at Rapaki (Fig. 5D,E). The ridgeline (i.e. volcanic source rock) to

https://doi.org/10.5194/nhess-2019-178
Preprint. Discussion started: 11 June 2019


Natural Hazards and Earth System Sciences
Discussions

the east obtains a maximum elevation of ~440 meters. Locally, individual vertical to subvertical bluff faces are estimated to be ~20-30 meters in height. From the base of the volcanic source rock, slopes extend downward toward Purau Bay at angles ranging from ~30° to ~5° near Camp Bay Road (Fig. 3). Field observations indicate the volcanic rock is overlain by loess, loess- and volcanic-colluvium, and pre-CES and CES rockfall boulders of small (e.g. <1 m^3) to extremely large size (e.g. >100 m^3). Deforestation of Purau slopes has left the hillside covered primarily in low-lying grass and bush. Shallow slips are abundant and are commonly observed on steep slopes, including valley flanks. Maximum landslide depth is typically ~1-1.5 meters and often exposes volcanic bedrock at bottom, indicating the overlying sediment is relatively thin. Tunnel gulley erosion predominates on canyon flanks and at lower elevations.

3 Methods

3.1 Field mapping and characterization of CES and pre-CES rockfall boulders

We mapped 1276 individual rockfall boulders at the Rapaki (pre-CES=408; CES=48) and Purau (pre-CES=684; CES=136) study sites for boulder volume ≥1.0 m^3 (see Supplementary Data, Tables S1-S4). Where safety conditions permitted, pre-CES and CES rockfall boulders were mapped to the base of the volcanic source rock. Location (latitude/longitude) and elevation (meters above sea level) were recorded for each rockfall deposit using a hand-held Garmin GPSMap 62s device. Boulder dimensions (i.e. height, length, width) were tape measured in the field. For pre-CES boulders partially buried to the degree that only two dimensions were adequately measurable, the shorter of the two measured lengths was used for the 3rd dimension, thus insuring a conservative boulder size estimate. No rounding factor was applied to volumetric estimations of pre-CES boulders. The lithology type was determined for each pre-CES boulder and was based primarily upon the observed dominant rock 'texture'. Boulder lithologies were categorized as VB or CL. Transitional lithologies were rarely observed (<1% of total) and assigned as VB or CL based on the volumetrically predominant rock type.

3.2 Boulder runout distance

https://doi.org/10.5194/nhess-2019-178
Preprint. Discussion started: 11 June 2019


Natural Hazards and Earth System Sciences
Discussions

Boulder runout distance was determined by measuring the shortest horizontal and ground-length distances, perpendicular to slope contour lines, from the nearest potential bedrock source areas to mapped boulder locations using Google Earth Professional (see Supplementary Data, Tables S5-S8). Runout distance was calculated for 409 pre-CES boulders and 48 CES boulders (for volume ≥ 1.0 m^3) at Rapaki. Due to safety concerns we were unable to record locations for pre-CES boulders within ~100 meters (map-length) of the volcanic source rock at this site. However, boulder frequency counts (for boulder volume ≥ 0.1 m^3) were field measured within a 300 m^2 area at distances of 0-10 meters (n=31), 30-40 meters (n=35), 60-70 meters (n=77), and 100-110 (n=24) meters from the volcanic source rock (see Appendix 1, Fig. A1). The boulder frequency counts at these distances were used to extrapolate the number of boulders across remaining sections of the study site, consistent with visual inspection of air photos. At Purau, four separate geomorphic domains (PD1-PD4) were created to evaluate pre-CES and CES boulder runout distance (see Fig. 3; Supplementary Tables S7, S8). The domains include interfluve and valley morphologies and target areas with both CES and pre-CES rockfall boulders, and cases where the pre-CES rockfalls were sourced from a single or limited number of rock exposures. We generally report map-length runout distance within this paper.

We used the empirical shadow angle method (Lied, 1977; Evans and Hungr, 1993) to analyze the travel distance of rockfalls at Rapaki and Purau. The shadow angle is the arctangent of the relationship Ht/Lt, where Ht is the height of fall on the talus slope (elevation difference between the apex of the talus slope and final emplacement location of the rockfall block) and Lt is the travel distance on the talus slope (horizontal distance between the apex of the talus slope and the final emplacement location of the rockfall block) (see Copons, 2009; Lied, 1977; Evans and Hungr, 1993) (see Appendix 1, Fig. A2). The shadow angle method is most suitable for our study (compared to the reach or 'Fahrboschung' angle) because it does not require identifying the source release location for individual rockfall blocks, a parameter we are unable determine for the pre-CES and CES rockfalls.

3.3 RAMMS rockfall modeling

Three model scenarios were conducted using the Rapid Mass Movements System (RAMMS) software (Bartelt et al., 2013; Leine et al., 2014). RAMMS_1 represents a bare-earth CES model and was performed to test the reliability of RAMMS in replicating the spatial

https://doi.org/10.5194/nhess-2019-178
Preprint. Discussion started: 11 June 2019


Natural Hazards and Earth System Sciences
Discussions

distribution for CES rockfalls at Purau. RAMMS_2 assumes a vegetated slope and simulates hillslope conditions prior to deforestation (i.e. prehistoric). RAMMS_3 models the potential future rockfall hazard at Purau and assumes a bare-earth (deforested) hillslope and dry soil moisture conditions to insure a worst-case (conservative) outcome. Please see Supp. Information for more detail on the individual RAMMS modeling scenarios.

The Purau terrain was modelled using a 4-m DEM (digital elevation model) derived from LIDAR (light detection and ranging) surveys to model CES (bare-earth scenario) and pre-CES prehistoric (forested slope scenario) rockfall distributions. The rockfall boulders were modelled as rigid polyhedral. The source areas (i.e. volcanic rock) and remaining runout terrain types (i.e. loess and loess/volcanic colluvium) (Appendix 2, Table A1 and Figs. A1-A3) for the RAMMS model scenarios (i.e. RAMMS_1, _2, _3) were chosen following the methods of Vick (2015) and Borella et al. (2016a) and delineated as polyline (Appendix 2, Figs. A2, A3) and polygon shapefiles (Appendix 2, Fig. A3) in ArcGIS from field observations, desktop study of orthophotography, and satellite imagery.

Boulder shape and size are highly influential in the dynamics and runout of a rockfall event (e.g. Leine et al., 2014; Latham et al., 2008). Boulder shapes and sizes used in the model simulations were representative of the true boulder geometries observed at Purau and Rapaki (Borella et al., 2016a). Rocks shapes were created using the RAMMS 'rock builder' tool, which creates boulder point clouds based on a user-defined shape and size. All boulder shapes reflected 'real' rock bodies that have been field-scanned. For each size class of boulder, varying shapes were selected, which are simplified to equant, flat, and long. Please see Supp. Information for more detail on boulder shape and size distributions utilized in each of the RAMMS modeling scenarios.

Vegetation was modelled in RAMMS as forest drag, a resisting force acting on the rock's center of mass when located below the drag layer height. The forest was parameterized by a drag coefficient, effective up to the input height of the vegetation layer. Typical values for the drag coefficient range between 100 and 10,000 kg/s (Bartelt et al., 2013; Leine et al., 2014). Vegetation was assigned an effective height of 10 m. A variable forest density was applied to account for the presumed denser vegetation (on average) within drainage valleys at the Purau study site (Appendix 2, Fig. A4). We assume more surface and subsurface water would be focused into topographic lows and would therefore promote denser tree growth. Within

https://doi.org/10.5194/nhess-2019-178
Preprint. Discussion started: 11 June 2019


Natural Hazards and Earth System Sciences
Discussions

drainage valleys a uniform drag force of 6000 kg/s was applied to each of the simulated boulders. Elsewhere at the study site, a drag force of 3000 kg/s was applied. These forest values are equivalent to those utilized in Borella et al. (2016a) at Rapaki in the Port Hills of southern Christchurch. We also simulated a uniform forest density increase of 10000 kg/s (see Results). As evidenced by modern native forest analogs, tree growth was extended upward to the base of the source rock and was also applied to areas between outcropping volcanic source rock.

3.4 Strong ground motions near rockfall source cliffs

Strong ground motion accelerograms for stations LPCC, D13C, D15C, and GODS were obtained from GeoNet (www.geonet.org.nz/, Fig. 6) to analyze the influence of ground motion on rockfalls. All these stations are Kinematrics Etna instruments except LPCC, which is a CUSP-3 instrument. LPCC recorded both Mw 6.2 event on 2011-02-21 and Mw 6 event on 2011-06-13. The other stations were installed following the Mw 6.2 earthquake and thus recorded only the Mw 6 earthquake. The data were sampled at 0.005 s (Nyquist frequency 100 Hz) and filtered with an effective passband having corners ~0.05 Hz and ~40 Hz. We integrated accelerograms to produce velocity seismograms and computed envelopes using ENV = sqrt[x(t)^2 + H(x(t))^2], where x(t) are time points in the seismogram and H is the Hilbert transform. The particle velocity hodograms are calculated in the horizontal plane by rotating the horizontal orthogonal components of the seismogram to a standard N-S E-W coordinate system. The time window of particle velocity hodograms is ± 5 s around the peak of the envelope of the east component. This ensures that the most significant ground motion resulting from both phase and group velocity peaks is accurately captured. Following a similar procedure, we computed particle motion hodograms by integrating accelerograms twice. These are given in Fig. 7 (A-E). Additional methods were used to analyse D13C data following interpretation of initial results; these are described in section 5.8.

4 Results

4.1 Rockfall mapping and boulder frequencies

4.1.1 Rapaki

https://doi.org/10.5194/nhess-2019-178
Preprint. Discussion started: 11 June 2019


Natural Hazards and Earth System Sciences
Discussions

315 A comparison of the spatial distributions for pre-CES and CES rockfalls at Rapaki (Fig. 2)
316 indicates that pre-CES rockfalls are more concentrated near the source area and have shorter
317 maximum runout distances (560±15 m) compared with the furthest travelled CES rockfalls
318 (700±15 m), which impacted the Rapaki village during the 2011 Christchurch earthquakes. The
319 CES rockfalls represent a subset of the pre-CES rockfall data set; the ratio of pre-CES (n=409)
320 to CES (n=49) rockfalls at Rapaki is ~8.5:1 (Fig. 2). The pre-CES and CES rockfall data sets
321 are separated into VB and CL boulders (Fig. 2, 4) to understand the influence of volcanic
322 lithology on rockfall runout and final resting location. Very few CL boulders with volume ≥1.0
323 m^3 exist for pre-CES (n=18) and CES (n=3) rockfalls at Rapaki. Pre-CES and CES VB boulders
324 display longer average and maximum runout distances than their CL counterparts (Fig. 2), and
325 CES CL and VB boulders display longer average and maximum runout distances compared
326 with their pre-CES equivalents. The ratio of pre-CES VB to CL and CES VB to CL rockfall
327 boulders is ~22:1 and ~15:1, respectively (Fig. 2).
328
329 **4.1.2 Purau**
330
331 Pre-CES and CES rockfalls are widely distributed at the Purau study location (Fig. 3). Rockfall
332 boulders are deposited on interfluves but are predominantly concentrated within nearby
333 canyons, highlighting the strong influence of topography at the site (Fig. 3). Seven (7) CES
334 detachment zones were identified in the field. CES rockfall boulders nearest to the Purau
335 village display the longest runout distance (372 m) and most distinct spatial contrast with
336 similarly sourced pre-CES boulders (deposited within ~105 meters of the local volcanic source
337 rock) (Fig. 3A). Elsewhere, pre-CES boulders can be observed at further distances from the
338 source rock than CES rockfalls. The ratio of pre-CES to CES rockfall boulders is ~5:1 (Fig.
339 3A). Pre-CES VB boulders are deposited throughout the Purau location, while the deposition
340 of CL pre-CES boulders is concentrated within the central and southern drainage canyons (Fig.
341 6A). The ratio of pre-CES VB to CL boulders is ~2:1 (Fig. 3B). CES VB boulders (n=127)
342 significantly outnumber CL boulders (n=9) at the Purau site (Fig. 3C), reflecting the lack of
343 detachment within CL source rock lithologies during the CES. The ratio of CES VB to CL
344 rockfall boulders is ~14:1 and represents a significance difference compared with the
345 corresponding pre-CES VB:CL ratio (Fig. 3C).
346
347 **4.2 Boulder morphology and other characteristics**

https://doi.org/10.5194/nhess-2019-178
Preprint. Discussion started: 11 June 2019


Natural Hazards and Earth System Sciences
Discussions

348

349 VB boulders (Fig. 4A-F) contain small to large porphyritic volcanic clasts that exhibit minor
350 to moderate vesicularity (up to ~10%) and are embedded within a finer crystalline and ash-
351 bearing matrix (see Fig. 4A,C,D,F). They are dominated by equant (all axes equal length)
352 shapes (see Fig.4C) although elongate (two short axes, one long) forms are observed. Flat (one
353 short, two long axes) morphologies are rare. VB pre-CES boulder surfaces show a high degree
354 of weathering and surface roughness (Fig. 4A-D,F). The surface roughness results from in-situ
355 differential weathering between the finer crystalline host matrix and more resistant embedded
356 volcanic clasts (see Fig. 4D). Surfaces show deep pitting, with amplitudes often exceeding 5-
357 10 centimeters in height. CL boulders (Fig. 4G-K) are more texturally homogenous, contain
358 fewer vesicles (estimated ~<1%) and exhibit a higher relative density (Carey et al., 2014;
359 Mukhtar, 2014). The pre-CES CL boulder surfaces exhibit low surface roughness (i.e. smooth
360 compared with VB boulders). Elongate and flat boulder morphologies predominate for CL
361 boulder lithologies (Fig. 4G-K).

362

363 Both VB and CL pre-CES boulders can be observed partially to nearly completely buried by
364 loess-colluvium (see Fig. 4A,B,G). Instances do occur, however, where no sediment is built-
365 up at the boulder backside (Fig. 4C) due to erosion (including tunnel gully formation). Burial
366 in hillslope sediment is most common for boulders located on midslope and footslope positions,
367 rather than those located on upper slope elevations, where erosion dominates. Pre-CES
368 boulders located in drainage canyons are subject to rapid deposition and erosion, and therefore
369 can be found without any sediment pile-up or preserving large colluvial wedges. VB boulders
370 preserve the thickest colluvial wedge sediments (see Fig. 4B).

371

372 **4.3 Source rock characteristics**

373

374 The volcanic source rock at Rapaki (Fig. 5A-C) and Purau (Fig. 5D,E) is comprised of
375 interlayered VB and CL layers (Fig. 5A-E). The breccia layers comprise the bottom and top of
376 discrete lava flows, while the coherent lava generally occupies the center of the lava flow where
377 cooling was not as rapid and there was less interaction with the substrate and/or cooling
378 interface (Fig. 5C-G). Jointing is pervasive within the volcanic source rock, but to varying
379 degree depending upon layer composition and corresponding texture. Layers comprised of CL
380 exhibit the highest fracture density (Fig. 5E,F) and were formed during primary cooling of the
381 lava flow, producing a columnar-style pattern. The CL layers contain numerous intersecting

https://doi.org/10.5194/nhess-2019-178
Preprint. Discussion started: 11 June 2019


Natural Hazards and Earth System Sciences
Discussions

382 sub vertical to vertical, to curvilinear joint sets, with spacing rarely exceeding ~1-2 meter. The
383 small joint spacing imparts a first-order control on CL boulder size and is reflected in the small
384 size range for pre-CES CL boulders. Layers comprised of VB exhibit a lower fracture density,
385 with joints more widely spaced (and irregular in shape), often 5-10 meters or greater apart (Fig.
386 5D,E). The wider spacing for joints within VB layers promotes greater rockfall boulder volume
387 (see Section 4.4. below).
388
389 During the CES, rockfall detachment occurred within approximately 9% (by area) of the
390 volcanic source rock overlying the Rapaki study hillslope (Fig. 5A). The volcanic source rock
391 is comprised of 86% VB and 14% CL. 69% of the detachment areas occurred within VB and
392 the remaining 31% within CL (Fig. 5A). However, 20% of the identified CL source rock
393 detached during the CES, while only 7% of the identified VB source rock detached during the
394 CES, indicating the CL lithology is more susceptible to detachment. Due to its significant size
395 and safety concerns, a similar characterization was not performed for the Purau volcanic source
396 rock.
397
398 **4.4 Boulder volume**
399
400 The size and frequency-volume distributions for pre-CES and CES rockfall boulders (for
401 volume ≥ 1.0 m^3) at Rapaki and Purau display similarity (Fig. 8A,C) and can be modeled using
402 power law functions (Fig. 8B,D), with the number of rockfall boulders decreasing significantly
403 as volume increases. Overall, statistical coherence is observed at the 25th, median, and 75th
404 percentile boulder sizes; however, pre-CES rockfalls are consistently higher for each of the
405 size categories at the two study locations (Table 1). Rapaki displays the highest pre-CES to
406 CES variance for 25th, median, and 75th percentiles, while Purau records the biggest pre-CES
407 to CES variance for the average, 95th percentile, and maximum boulder volumes (Table 1, Figs.
408 8A,C).
409
410 At Rapaki, VB pre-CES and CES boulder volumes display a similar trend (Fig. 8E) compared
411 to the pre-CES and CES boulders (see Fig. 8A), indicating the dominance of VB boulders for
412 volume ≥1.0 m^3. Pre-CES VB boulders display higher volumes in each of the size categories,
413 particularly for median and maximum boulder sizes (Table 2). Pre-CES CL boulders display
414 consistently higher values for each of the size categories with the exception of the 75th

https://doi.org/10.5194/nhess-2019-178
Preprint. Discussion started: 11 June 2019


Natural Hazards and Earth System Sciences
Discussions

415 percentile (Fig. 8E, Table 2). At Purau, CES VB and CL boulders exhibit a smaller distribution
416 of boulder sizes compared with their pre-CES equivalents (see Fig. 8F). Pre-CES VB and CL
417 boulders are higher in each of the size categories (Table 2, Fig. 8F), with the exception of the
418 median boulder size, where the CES CL median boulder volume is slightly more than the pre-
419 CES CL value (Table 2). It is notable that the highest percent (%) variance in boulder volume
420 between pre-CES and CES boulders is recorded with the Purau VB boulders (Table 2); the
421 only exception is for maximum boulder size, where the percent (%) difference between Purau
422 CL pre-CES and CES boulders is even greater (Table 2).
423
424 The volume and frequency ratios for pre-CES and CES rockfall boulders are plotted in Figure
425 9A. The pre-CES to CES boulder volume ratios at Rapaki and Purau range from ~8-12 and ~7-
426 37, respectively (Table 3A, Fig. 9A). The corresponding frequency ratios are consistently
427 lower, ranging from ~6-8.5 and ~3.5-27.5 (Table 3A, Fig. 9A). Overall, the boulder volume
428 and frequency ratios are greater at Rapaki, with the exception of the CL lithology (Tables 3B,
429 3A, and Fig. 9A).
430
431 The calculation of VB and CL boulder percentages at Rapaki for pre-CES and CES rockfalls
432 indicates that VB boulders comprise ≥ 98% by volume and ≥ 94% by frequency (n) for all
433 Rapaki conditions, while at Purau the corresponding percentages are ≥ 90% (volume) and
434 ≥64% (frequency) respectively (Table 3B). All of the lowest VB percentages exist at the Purau
435 study location (see Table 3B, individual domain data).
436
437 **4.5 Boulder runout distance**
438
439 The frequency-runout distance distribution for pre-CES boulders at Rapaki can be
440 characterized by power and exponential laws (Fig. 9B), with the number of rockfall boulders
441 with long runout distances decreasing dramatically with increasing distance from the volcanic
442 source rock. The exponential regression is best fit to the entire data set (including extrapolated
443 boulders within 100 m of source rock), while the power law displays the strongest fit for the
444 mapped rockfall boulders (Fig. 9B). CES rockfalls display a poor exponential fit and do not
445 indicate a similar inverse relationship between boulder frequency and runout distance (Fig.
446 9B). The frequency-runout distribution for CES rockfalls indicates that the number of boulders
447 remains more or less consistent regardless of distance from the source rock. Using the shadow

https://doi.org/10.5194/nhess-2019-178
Preprint. Discussion started: 11 June 2019

448 angle method we plot travel distance on the talus slope (Lt) versus height on the talus slope
449 (Ht) with a fitted polynomial regression line (Fig. 9C). The correlation coefficient is 0.9699 for
450 CES rockfalls and 0.9717 for pre-CES rockfalls (Fig. 9C). The minimum shadow angle for
451 pre-CES is 25°, while the minimum shadow angle (for the furthest traveled CES rockfall
452 boulders) is 23°. At Rapaki, the maximum runout distance for pre-CES and CES VB boulders
453 exceeds the furthest travel distances for pre-CES and CES CL boulders, respectively (Table 4).
454 The CES VB boulders exceed pre-CES VB runout by ~165 meters and CES CL boulders
455 exceed CL pre-CES runout by ~138 meters (Fig. 2A,B; Table 4).
456
457 At Purau, Lt versus Ht is plotted for four (4) separate geomorphic domains (PD1-PD4) to
458 evaluate the distribution of pre-CES and CES boulder runout distances (Fig. 9D; see Fig. 3 for
459 domain locations). The pre-CES and CES rockfalls for the individual domain data sets are
460 characterized by a variety of regression functions with high correlation coefficients (Fig. 9D;
461 Supplementary Data, S24). CES rockfalls in PD1 and PD4 have significantly further maximum
462 runout distances than their pre-CES counterparts, while the inverse is evident in PD2 and PD3.
463 [We note that only two CES boulders were observed in PD2.] The minimum shadow angle for
464 pre-CES rockfalls at Purau is 25°, while the corresponding minimum CES rockfall shadow
465 angle is 18°. At Purau, the longest recorded runout distances occur for pre-CES CL and VB
466 boulders and CES VB rockfall boulders within PD3 (Table 4).
467
468 At Rapaki, no relationship has been obtained plotting individual boulder volumes and the
469 tangent of the shadow angle (Fig. 9E). A wide range of boulder sizes are evident for the full
470 spectrum of pre-CES and CES rockfall runout distances by means of the shadow angle. The
471 same is largely true at Purau, where correlations for the individual domains (PD1-PD4) are
472 poor and the data has a high degree of scatter (i.e. low correlation coefficients); although the
473 data does show a slight negative relationship between block volume and *Ht/Lt* ratio value (that
474 is, a slight increase in runout distance as boulder size increases) (Fig. 9F).
475
476 **4.6 RAMMS rockfall modelling**
477
478 **4.6.1 RAMMS_1**
479
480 Final resting locations (n=1072) are generated for simulated rockfalls released from the seven
481 (7) field-identified CES detachment zones at Purau (labeled CES-1 through CES-7) (Fig. 10A).

https://doi.org/10.5194/nhess-2019-178
Preprint. Discussion started: 11 June 2019


Natural Hazards and Earth System Sciences
Discussions

The empirical CES boulder locations are depicted as red circles. RAMMS_1 (bare-earth CES model scenario) is successful in replicating the overall spatial pattern for detached and distributed CES rockfalls at Purau for locations CES-3, -4, -5, -6, and -7. Below the CES-7 source rock, RAMMS maximum runout distances (~370 m) are well matched to the maximum travel distance for mapped CES rockfalls (~357 m). Maximum runout distances for the RAMMS boulders are overestimated at CES-1 and CES-2 (Fig. 10A). We note that only 2 boulders were released at CES-1 during the CES and were deposited within ~12 meters of the source rock. RAMMS_1 effectively captures the lateral dispersion for the mapped CES boulders at CES-2, CES-3, and CES-4, but overestimates this effect within the CES-5 and CES-6 valleys, and slightly underestimates the lateral dispersion of CES rockfalls beneath CES-7.

4.6.2 RAMMS_2

The RAMMS_2 model scenario (forested hillslope) is moderately successful (slight overprediction) in replicating the overall spatial distribution and maximum runout distances for the majority of mapped pre-CES rockfalls at Purau (Fig. 10B). The exception is area CES-7, where RAMMS predicts deposition of pre-CES boulders significantly farther (~325 m) from the source rock than is evident in the field (~80 m). Elsewhere, the greatest variance in maximum runout distance between RAMMS_2 and the mapped pre-CES boulders is ~75-100 m (see Fig. 10B). An increase in forest density to 10,000 kg/s, spread uniformly across the study site produces the best fit to the pre-CES boulder spatial distributions (in particular, maximum runout distance) (see Figure 10B, white dashed line). RAMMS_2 successfully models the lateral dispersion for the mapped pre-CES boulders (with the exception of area CES-7) (Fig. 10B). The RAMMS_2 model scenarios identify pre-CES rockfall boulders that have likely experience post-emplacement mobility (see Fig. 10B). Note the collection of pre-CES boulders within the central drainage canyon that exceed the limit of simulated RAMMS boulders (Fig. 10B). Field observations confirm that boulder depositional patterns beyond the limits of the final resting locations for RAMMS simulated rockfall boulders are consistent with deposition by debris flow and other transport/deposition processes. Importantly, we observe no mapped pre-CES boulders outside of the valleys that exceed the RAMMS_2 simulated maximum runout distances.

4.6.3 RAMMS_3

https://doi.org/10.5194/nhess-2019-178
Preprint. Discussion started: 11 June 2019


Natural Hazards and Earth System Sciences
Discussions

RAMMS_3 models the potential future rockfall hazard at Purau and assumes a bare-earth (deforested) hillslope and dry soil moisture conditions to insure a worst-case (conservative) outcome (Fig. 10C). As expected, RAMMS_3 rockfalls obtain higher kinetic energy, velocity, and jump heights than RAMMS_2 boulders (see Supplementary Data, S18, S19), and as a result, runout farther than the RAMMS_2 boulders (Fig. 10B). On average, maximum runout distance for RAMMS_3 boulders is ~450-500 m, representing an increase of ~100-150 m compared with RAMMS_2 boulders, a difference consistent with results from RAMMS numerical modeling at Rapaki (see Borella et al., 2016a). The RAMMS_3 results indicate that the existing residence furthest to the north (S1) (Fig. 10C) and potential development at S2 could be adversely impacted by future rockfall events. With the exception of area CES-7, RAMMS_3 maximum runout distances are well in exceedance of the mapped locations for the CES rockfall boulders (Figs. 10A,C) and highlights the potential input from additional detachment sites within the Purau volcanic source rock.

4.7 Strong ground motion data

High frequency data show complex velocity and displacement paths for any given site. The variations across the sites are significant, and they have been reported previously (Van Houtte et al., 2012; Bradley, 2016). Even for the same site (LPCC, Fig. 7A,B), particle velocity and motion hodograms show different polarization characteristics for different earthquakes. Peak velocities and displacements recorded at LPCC site are higher for the Mw 6.2 than the smaller event Mw 6.0 (Fig 7A, B). The observed inter-site and inter-event variations in polarization of peak velocities and displacements can be attributed to source radiation pattern (Lee, 2017) and complex wave propagation effects such as scattering. For instance, simulating high frequency (> 1 Hz) 3-D wavefields, Takemura et al. (2015) showed that near-station irregular topography amplifies scattering of seismic wavefield, producing long coda and distortions to P wave polarizations. This is not surprising given that Fresnel volume – the region to which a transmitting seismic wave is sensitive – is inversely related to wave frequency (Spetzler and Snieder, 2004), due to which near-station geological conditions modify wave characteristics at high frequencies. The control of near-station geology over polarization and amplification characteristics at high frequencies (Bouchon & Barker, 1996) reduces our ability to extrapolate these characteristics to distant sites.

5 Discussion

https://doi.org/10.5194/nhess-2019-178
Preprint. Discussion started: 11 June 2019

550
551 **5.1 Rockfall spatial distributions and frequencies**
552
553 At Rapaki, significant differences in spatial distribution between the pre-CES and CES boulder
554 populations are observed (Fig. 2 and Table 4). The increased distance for the CES rockfall
555 boulders is interpreted as an effect of anthropogenic deforestation on the hosting hillslope,
556 which enabled CES boulders to travel further than their pre-CES counterparts due to reduced
557 resistance from vegetation (Borella et al., 2016a). The increase in CES runout distance
558 (~165±15 m) (and corresponding reduction in minimum shadow angle) resulted in significant
559 impact and damage to homes and infrastructure in the Rapaki village, and highlights the
560 importance of considering the effects that modifications to hillslopes may have on rockfall
561 hazard. At Rapaki, pre-CES VB boulders are present in significantly greater number and have
562 further average and maximum runout distances than the pre-CES CL boulder lithologies (Fig.
563 2A, Table 4). A similar relationship is evident between the CES VB and CL boulders, where
564 CES boulders with the furthest runout distances are exclusively comprised of volcanic breccia
565 (Fig. 2B). It is possible that the reduced runout distances for pre-CES and CES CL boulders is
566 a statistical counting bias (i.e. low number of CL boulders for volume ≥1.0 m^3), but a more
567 plausible explanation is that the reduced runout distance for CL boulder lithologies is a result
568 of CL boulder shapes being dominated by elongate and flat morphologies (Fig. 10A-F), which
569 would have more difficulty traveling downslope.
570
571 At Purau, discerning the differences in spatial distribution between pre-CES and CES rockfalls
572 is more difficult, primarily due to the topographic forcing of rockfalls into nearby drainage
573 valleys and post-emplacement mobilization (Fig. 3). Location CES-7 (furthest southern
574 rockfalls) does show a similar pre-CES:CES spatial scenario to Rapaki, with CES boulders
575 traveling significantly further than their pre-CES equivalents (see Fig. 5); a discrepancy which
576 could also be attributed to intervening deforestation on the hillslope. However, elsewhere at
577 the Purau field site inverse spatial scenarios are evident, with pre-CES boulders deposited
578 further from the source rock than their CES counterparts (see Fig. 2A, Table 4). This is
579 primarily observed within drainage valleys where field observations suggest pre-CES boulders
580 have been remobilized (debris flows, floods) and carried further from the source rock following
581 their initial emplacement.
582

https://doi.org/10.5194/nhess-2019-178
Preprint. Discussion started: 11 June 2019


Natural Hazards and Earth System Sciences
Discussions

583 The CES rockfall boulders at both sites represent a subset of the larger pre-CES rockfall
584 database, suggesting the preservation of multiple pre-CES rockfall events. The ratio for the
585 number of pre-CES to CES rockfall boulders is higher at Rapaki (~8.5:1) than Purau (~5:1)
586 (Table 3, Figs. 2, 3). One cause of the observed difference may be the higher number of CL
587 boulders with size ≥1.0 m^3 at the Purau study site (Fig. 8E,F). At Rapaki, most of the
588 detachment within the CL source rock generated boulder volumes below the 1.0 m^3 threshold.
589 As a result, the ratio of pre-CES VB:CL boulders is significantly higher at Rapaki (~22:1)
590 (Table 3B, Fig. 2A) than Purau (~2:1) (Table 3B, Fig. 3B). This contrasts with the ratio of CES
591 VB:CL boulders at Rapaki (~15:1) (Table 3B, Fig. 2B) which shows near equivalence to Purau
592 (~14:1) (Fig. 3C). The CES VB:CL ratio at Purau is more consistent with our field observations
593 where VB predominates in the source rock. Overall, the results indicate there is a high degree
594 of lithologic variation and discontinuity spacing (e.g. joints) within the source rock and
595 suggests the cumulative ratio of VB:CL boulders can be significantly different from that
596 generated locally during a single rockfall event.
597
598 **5.2 Boulder morphology and other characteristics**
599
600 It is well-established that boulder morphology (shape) plays a primary role in the spatial
601 distribution of the rockfalls (e.g. Leine et al., 2014). The shapes for the VB (Fig. 4A-E) and
602 CL (Fig. 4G-K) boulders are primarily controlled by pre-existing discontinuities in the source
603 rock; in particular, jointing. We modeled the influence of boulder shape on spatial distribution
604 for the VB and CL lithologies assuming detachment from the CES-7 site (under bare-earth
605 conditions) using RAMMS (Fig. 11). To eliminate the effect of boulder size, a volume of 1.0
606 m^3 was assumed for all rockfall boulders. The VB boulders were assigned a range of equant
607 boulder shapes, while CL boulders were assigned only elongate and flat boulder morphologies.
608 The model results highlight the differences in boulder spatial distribution resulting from
609 differences in boulder shape, with equant (VB) boulder lithologies displaying a significantly
610 higher relative percentage of longer runout distances (Fig. 11A) compared with the
611 elongate/flat (CL) boulder morphologies (Fig. 11B). We recognize that the modeling represents
612 an ideal scenario (i.e. other transition morphologies do exist for the VB and CL boulders) and
613 was conducted primarily to provide a sense for the expected spatial patterns assuming the
614 distinct VB and CL boulder shapes. Further work is required to verify coherence between field
615 observations and model results.

https://doi.org/10.5194/nhess-2019-178
Preprint. Discussion started: 11 June 2019


Natural Hazards and Earth System Sciences
Discussions

616

617 **5.3 Source rock characteristics**

618

619 We combined high-resolution aerial photography (from UAV) with field observations to
620 characterize the Rapaki source rock. The volcanic source rock is comprised of 86% VB and
621 14% CL (VB:CL ratio=~6:1) (Fig. 5A-C) by percent area, values that are lower than the
622 corresponding VB and CL percentages determined from rockfall frequency and volume for the
623 pre-CES (96% VB and 4% CL) and CES (94% VB and 6% CL) rockfalls. We attribute the
624 percent differences between source rock and rockfalls to the influence of the larger VB boulder
625 sizes and the lower number of CL rockfalls meeting the ≥ 1.0 m^3 size threshold. These two
626 factors also explain detachment during the CES, where 69% of the detachment areas occurred
627 within VB and the remaining 31% within CL (Fig. 5A-C), yielding a lower VB:CL ratio of
628 ~2:1 compared with the corresponding boulder volume and frequency ratios (~15:1 and ~52:1,
629 respectively) (Table 3B). Comparisons between volcanic source rock characteristics and
630 boulder volumes (VB and CL) are discussed in Section 5.4. (see below).

631

632 We were unable to conduct a similar source rock investigation at Purau because the size of the
633 source rock was too great and in several cases deposition of rockfall boulders into discrete
634 geomorphic domains resulted from detachment on multiple source rock outcrops. However,
635 observations were made for the Purau source rock (Fig. 5D,E) as well as other volcanic coastal
636 cliff outcrops at Sumner (Fig. 5F) and Red Cliffs (Fig. 5G). Field observations indicate CL
637 layers at Purau are not as prevalent as (and generally thinner than) VB layers, but in some cases
638 may exceed a thickness of 5 meters, which is thicker than CL layers observed at Rapaki (see
639 Fig. 5B,C). At Sumner and Redcliffs, VB and CL layers display roughly equivalent thicknesses
640 (~2-3 m), a condition not apparent at Rapaki or Purau. The variability in layer thickness
641 presumably reflects differences in proximity to source vents and differing conditions during
642 primary cooling of the lava flows.

643

644 **5.4 Boulder volume**

645

646 The size and frequency-volume distributions for pre-CES and CES rockfalls at Rapaki (Fig.
647 8A,B) and Purau (Fig. 8C,D) can be modeled using a power law and indicate a predictable
648 decrease in the number of boulders as boulder volume increases. A power law frequency-size

https://doi.org/10.5194/nhess-2019-178
Preprint. Discussion started: 11 June 2019


Natural Hazards and Earth System Sciences
Discussions

649 distribution is well-established (e.g. Dussauge-Peisser et al., 2002; Guzzetti et al., 2002) for
650 rockfalls globally and has also been successfully applied for CES rockfalls in Banks Peninsula
651 (Massey et al., 2014). At both study locations, pre-CES rockfalls exceed the size of their CES
652 counterparts in all statistical categories (Table 1). The net increase in volume distribution for
653 pre-CES boulders could represent a statistical effect and reflect the inclusion of more boulders
654 into the rockfall data set through time (which would increase the likelihood of more large
655 boulders) and/or could reflect higher shaking intensities and/or source rock vulnerability during
656 pre-CES events.
657
658 A comparison of rockfall volumes between the two sites indicates that pre-CES rockfalls at
659 Rapaki are greater for the 25th, median, and 75th percentile sizes (Table 1) while Purau exhibits
660 larger sizes for the 95th percentile, maximum, and mean boulder categories (Table 1). For CES
661 boulders, the 25th, median, 75th, and 95th percentile Rapaki CES boulders are slightly larger
662 compared with Purau CES boulders, while the maximum and mean boulder size categories are
663 higher at Purau (Table 1). Although differences are evident, the overall size distributions are
664 comparable (Table 1). Variations in CES vs. pre-CES boulder volumetric distributions for the
665 same lithologies could reflect structural and/or more subtle lithologic variability within the
666 source cliffs from which boulders were derived, and/or post-detachment weathering during
667 boulder transport or *in situ*.
668
669 The volume for pre-CES and CES VB boulders is significantly larger than the corresponding
670 CL boulders at Rapaki (Fig. 8E, Table 2) and Purau (Fig 8F, Table 2), reflecting the
671 predominance of VB within the source rock and wider joint spacing within the thicker VB
672 layers. As expected, the pre-CES VB and CL boulder sizes exceed those of their CES
673 equivalents, with the exception of the 75th percentile CL boulders at Rapaki and median CL
674 boulders at Purau (Table 2, Figs. 8E,F). It is notable that the largest percent variance between
675 pre-CES and CES boulder size occurs for the Purau VB boulders (with the exception of
676 maximum boulder size) (Table 2). We are uncertain why this difference is greatest within the
677 Purau VB boulders, but could reflect a smaller joint spacing at the CES VB detachment sites.
678
679 **5.5 Boulder runout distance**
680
681 The frequency-runout distance distribution for pre-CES boulders at Rapaki can be modeled
682 using a power law and exponential fit. The exponential law fit (Fig. 9B, short dashed line)

https://doi.org/10.5194/nhess-2019-178
Preprint. Discussion started: 11 June 2019


Natural Hazards and Earth System Sciences
Discussions

683 includes all data points (including extrapolated data within 100 m of source rock) and
684 highlights the importance of slope and initial impact velocity at the cliff base, which causes
685 more boulders to be deposited at greater distances and creates a deviation from the power law
686 fit (Fig. 9B, solid line). The exponential fit for CES rockfall boulders is poor and indicates
687 there is no discernable correlation between CES boulder frequency and runout distance (Fig.
688 9B, long dashed line). Despite the low number of CES boulders (n=48), it is interesting that
689 the CES runout distribution shows such a noticeable deviation from the pre-CES data set and
690 could reflect the influence of deforestation on runout distance. This would imply that the
691 incremental input of CES and future rockfalls at Rapaki (emplaced during bare-earth
692 conditions) will modify the overall trend for the cumulative rockfall data set.
693
694 At Rapaki, the shadow-angle *Ht/Lt* relationship is fit best using a polynomial regression (Fig.
695 9C). The trend indicates a positive correlation between talus slope height (Ht) and travel
696 distance on the talus slope (Lt), with a reduction in the rate of increase as rockfall runout (Lt)
697 increases. At Purau, CES and pre-CES rockfalls (within individual geomorphic domains) are
698 modeled using a variety of data functions (e.g. linear, log, polynomial), suggesting intra-site
699 geomorphic and geologic factors affecting rockfall hazard are spatially variable **(**Fig. 9D**)**. We
700 note that Copons (2009) reports linear regression lines for historical rockfalls in the Central
701 Pyrenees using the shadow-angle method, and locally, Massey et al. (2014) also show linear
702 regression fits using the shadow-angle method for CES rockfalls in the Port Hills of southern
703 Christchurch. Our data indicates that non-linear regression functions (for the shadow-angle
704 method) are more successful in capturing the Ht/Lt relationship as distance from the source
705 rock increases.
706
707 No clear relationship is obtained between boulder volume and runout distance at Rapaki (Fig.
708 9E) and Purau (Fig. 9F). At both sites, a wide range of boulder sizes exist for the full spectrum
709 of pre-CES and CES *Ht/Lt* ratios, suggesting that boulder size is not a primary driver for runout
710 distance at the study sites; although it is possible that smaller boulders (e.g. ~1-2 m^3) exhibiting
711 long runout distances (i.e. low *Ht/Lt* ratios) may represent smaller rock fragments detached
712 from larger boulders during transport and eventual emplacement on the hillslopes and within
713 valleys.
714
715 **5.6 RAMMS rockfall modelling**
716

https://doi.org/10.5194/nhess-2019-178
Preprint. Discussion started: 11 June 2019

5.6.1 RAMMS_1

A primary challenge in replicating the distribution of CES rockfalls was determining an appropriate set of terrain parameters for the drainage valleys (see Appendix 1, Table A1). To match the RAMMS boulders with the field-mapped CES rockfalls (Fig. 10A) it was necessary to create separate valley terrain polygons and modify the terrain parameters to reflect the high degree of impedance and/or dampening (Vick et al., 2019) in the drainage gullies (see Appendix 2, Table A1). Our field observations confirm the presence of abundant pre-existing boulders within drainage valleys (Fig. 12A-F) and many instances where CES boulders were stopped by pre-CES rockfalls (see Fig. 12A-C). The effect of pre-CES rockfall debris on boulder transport and final resting location needs to be further investigated in order to effectively model impediments within drainage valleys. Further, a more refined understanding for the influence that substrate soil moisture content has on rockfall runout is required (Vick et al., 2019). We note that the DEM used for our study has a resolution of 4 m and may not adequately simulate the smaller scale surface roughness (e.g. clustering of boulders below this size threshold) observed during our field studies (Fig. 12A-G).

5.6.2 RAMMS_2

The RAMMS_2 model scenario (prehistoric/forested hillslope) is moderately successful (slight overprediction) in replicating the overall spatial distribution (including maximum runout distances) for the majority of mapped pre-CES rockfalls at Purau (Figs. 10B). The best fit occurs when the forest density is increased to 10000 kg/s (dense vegetation) and applied uniformly across the Purau hillslopes (see Figure 10B, white dashed line). This represents an increase compared with the forest density used at Rapaki (i.e. 3000 kg/s for moderate vegetation [interfluves], 6000 kg/s for dense vegetation [valleys] (see Borella et al., 2016a) and implies that vegetation may have been denser on the northwest-facing Purau hillslopes compared with the south/southeast facing Rapaki hillslope.

We note the difference between maximum runout distance for RAMMS and empirical pre-CES boulders at the CES-7 site (Fig. 10B). RAMMS predicts that pre-CES boulders should be deposited further from the source rock (maximum runout distance=~325 m) than is observed (maximum runout distance=~105 m) in the field. Several possible explanations exist including: (1) pre-CES boulders were in fact deposited further from the source rock and were

https://doi.org/10.5194/nhess-2019-178
Preprint. Discussion started: 11 June 2019


Natural Hazards and Earth System Sciences
Discussions

751 subsequently buried by loess and hillslope colluvium; (2) RAMMS underestimates the effect
752 of hillslope vegetation during prehistoric times; (3) during pre-CES times less of the source
753 rock was exposed (due to burial) and therefore the volcanic rock was less susceptible to
754 detachment during shaking; and/or (4) during pre-CES shaking events the direction of strong
755 ground shaking was not favourable to rockfall detachment. (5) Scenario 1 is possible but would
756 need to be confirmed through subsurface trenching or ground penetrating radar (GPR)
757 methods. Tunnel gulley erosion has exposed sections of the subsurface on the CES-7 hillslope
758 and no buried boulders are evident. Scenario 2 is probable based on our observations of forested
759 hillslopes elsewhere in the Port Hills and greater Banks Peninsula area. It is common for dense
760 native vegetation to grow up to, and in some cases, onto portions of the volcanic source rock.
761 In these cases, a high volume of detached rockfalls are stopped adjacent to the source rock and
762 never generate the required momentum to runout an appreciable distance. Scenario 3 is also a
763 possibility and requires that the CES-7 source rock was partially buried during emplacement
764 of the pre-CES rockfalls. The last phase of hillslope aggradation would have occurred during
765 the last glacial maximum (~18-24 ka) and possibly up to ~12-13 ka (see Borella et al., 2016b).
766 We assume the Purau hillslopes have been net erosional (i.e. downwasting) since the early
767 Holocene; a condition that would have been significantly accelerated after deforestation in the
768 Purau area. Option 4 is a final possibility but would require that the ~north facing PD1 source
769 rock is oriented in such a way that strong ground motions from multiple prehistoric shaking
770 events were unable to create rockfall detachment to the degree evident in the CES (see section
771 5.7 for more discussion on strong ground motions).
772
773 RAMMS 2 model scenarios effectively identify pre-CES rockfall boulders that have likely
774 experience post-emplacement mobility (Fig. 10B). This is shown by the collection of pre-CES
775 boulders within the central drainage canyon that exceed the limit of simulated RAMMS
776 boulders (Fig. 10B), indicating a transport mechanism other than rockfall. Field observations
777 confirm that the depositional patterns of boulders located beyond the limits of what RAMMS
778 predicts are consistent with debris flow and other transport/deposition processes. This is further
779 highlighted by the numerous and large pre-CES rafted boulders (maximum volume=20 m^3)
780 identified near the Purau coastline (see Fig. 3).
781
782 Finally, we observe no mapped pre-CES boulders outside of the valleys that exceed the
783 RAMMS_2 maximum runout distance (Fig. 10B), implying that the mapped pre-existing
784 boulders (yellow circles) were deposited prior to deforestation of the Purau hillslopes and are

https://doi.org/10.5194/nhess-2019-178
Preprint. Discussion started: 11 June 2019


Natural Hazards and Earth System Sciences
Discussions

785 prehistoric (i.e. deposited prior to European arrival) in age. This result is consistent with
786 prehistoric boulder ages determined at the Rapaki study site where the youngest emplacement
787 ages for pre-CES boulders are ~2-6 ka (Mackey and Quigley, 2014; Borella et al., 2016b).
788
789 **5.6.3 RAMMS_3**
790
791 With the exception of area CES-7, RAMMS_3 maximum runout distances are well in
792 exceedance of the mapped locations for the CES rockfall boulders (Fig. 10C), and highlights
793 the potential increased rockfall hazard resulting from input from additional detachment sites,
794 particularly those overlying hillslopes where boulder trajectories are not as strongly influenced
795 (i.e. captured) by nearby valleys. The results indicate that development at S1 and S2 sites could
796 be adversely impacted by future rockfall events (Fig. 10C). Assuming terrain characteristics
797 remain similar, Sites 3, 4, and 5 are unlikely to be impacted by rockfall boulders in the future,
798 although additional mapping and related structural studies of the volcanic source rock is
799 required to determine the most vulnerable rockfall source areas.
800
801 **5.7 Interpretations of strong ground motion data**
802
803 Preceding studies provide some insight into possible strong ground motion characteristics at
804 Rapaki and Purau during the Mw 6.0 and 6.2 earthquakes. Kaiser et al.'s (2014) seismic array
805 analysis of weak ground motion provides information regarding frequency-dependent
806 amplification at Kinsey Terrace, Redcliffs, and Mt. Pleasant (henceforth Ksites), all of which
807 are north-facing slopes in the Port Hills. They found that both morphological features as well
808 as properties of the wave propagation media control frequency-dependent amplification. In
809 particular, significant ground motion amplification was observed at 1 – 3 Hz frequency range
810 on top of narrow, steep-sided ridges. At these low frequencies (f), seismic wavelengths (λ) are
811 comparable to ridge width of Ksites. Therefore, seismic waves in the 1 – 3 Hz frequency band
812 appear to excite natural resonance (or natural frequency; f_n), optimizing ground motion.
813
814 It is interesting to evaluate the implications of Kaiser et al.'s (2014) low frequency observations
815 to Rapaki and Purau rockfall sites. Both these sites are located at higher elevations than Ksites.
816 Thus, their ridge width (~400 – 500 m) is somewhat less than that at Ksites (~ 600 – 1000 m).
817 Using this information, we estimate f_n to be < 5 Hz (see supp infor).

https://doi.org/10.5194/nhess-2019-178
Preprint. Discussion started: 11 June 2019


Natural Hazards and Earth System Sciences
Discussions

Whether ground motion with f_n was excited at these sites depends on the amount of energy carried by seismic waves in that frequency band. This information is contained in the spectra of velocity seismograms – a proxy for kinetic energy distribution over frequency. We selected D13C station for this preliminary analysis because the distance between this station and the Rapaki site is only about 2 km. They are also at similar elevations with ridge morphologies resembling each other. Rapid variations in geological conditions are unlikely over such short length-scales, which allows us to extrapolate both high and low frequency wave characteristics observed at D13C station to Rapaki with less uncertainty than the other stations. The nearest station to Purau is LPCC (~ 5 km). The two sites are vastly different as LPCC is located at the toe of a steep cliff in the Lyttelton Port, whereas Purau sites are high elevation ridges. Thus, ground motion recorded at LPCC is not a reliable proxy for ground motion characteristics at Purau. The next nearest station D15C is ~ 7 km from Purau and it suffers from morphological dissimilarities (variations in ridgeline orientation and morphology) that make extrapolating ground motion between the sites highly unreliable. Despite the fact that D13C station is located ~10 km from Purau, similarity of morphological features including elevation makes D13C a desirable station to understand ground motion at Purau.

We computed velocity spectra of east and north components of the station D13C (Fig. 13) to qualitatively assess seismic energy transmission through our rockfall sites. We find that the transition from the flat spectrum to a rapid fall off occurs at ~3 – 4 Hz. This means that the 2011-06-13 Mw 6 earthquake carried most of its energy at frequencies less than ~3 – 4 Hz. Together with our estimates of f_n (< 5 Hz), we can thus infer that the passage of seismic waves excited natural resonance at Rapaki and Purau sites. The combined effects of natural resonance and wave focusing towards the ridge crest (Hartzell et al., 1994; Bouchon & Barker, 1996) in these hard rock sites have the potential to optimize shaking, promoting rockfalls.

It is interesting to note, however, that D13C recorded the lowest peak velocities (223 mm/s and 178 mm/s) and displacements (38 mm and 74 mm) of the four stations considered here (Fig. 7C). Out of these stations, it is also the only station that recorded no acceleration above 0.3g on any component. These features of the wavefield are not surprising because distance from D13 C to epicentre of the Mw 6 earthquake is twice (~9 km) as large as that from the other stations (~4.5 km). For this reason, it is likely that other possible effects (e.g., rockmass weakening by prior CES earthquakes), in addition to strong ground motions from the Mw 6

https://doi.org/10.5194/nhess-2019-178
Preprint. Discussion started: 11 June 2019


Natural Hazards and Earth System Sciences
Discussions

852 earthquake, were responsible for triggering major rockfalls at the study sites. Unfortunately,
853 D13C was not in operation at the time of these previous larger earthquakes to assess severity
854 of ground motion. Nonetheless, records from stations closest to D13C indicate that those sites
855 have exceeded the 0.3g peak ground acceleration (PGA) threshold important for engineering
856 considerations. For instance, LPCC station located ~6 km from D13C recorded 0.3g and 0.9g
857 PGA following the Mw 7.1 and Mw 6.2 events respectively (Bradley & Cubrinovski, 2011).
858 Moreover, extrapolation of PGA contours of Bradley (2012) suggests that D13C and Rapaki
859 sites experienced PGA exceeding 0.25g and 0.45g during Mw 7.1 and Mw 6.2 earthquakes
860 respectively. Some of the rockfall sites investigated herein might have had reached a critical
861 failure threshold prior to being triggered by the 2011-06-13 Mw 6 earthquake.
862
863 The particle velocity and motion hodograms (Fig. 7A-E) we computed also carry directional
864 information of particle behaviour in addition to intensity that we discussed earlier. Past studies
865 show that seismic wave polarizations are amplified in directions perpendicular to fracture
866 surfaces, weakening the coherence between outer blocks of rock with bedrock during the
867 passage of a seismic wave (Kleinbrod et al., 2017; Burjánek et al., 2018). If blocks of rock are
868 primed for failure by previous events, this effect can produce rockfalls at a local magnitude as
869 small as ~4 (Keefer, 1984). The velocity hodogram of D13C exhibits a strong ENE-WSW
870 component. Note that this direction makes roughly ~30º to ~60º angle with rock faces at PD2,
871 PD3, PD4, and RAP sites (Fig. 7C). Thus, it is reasonable to assume that particle velocities in
872 this dominant direction are favourable for triggering rockfalls particularly if the rock faces were
873 primed for failure. The angle between this dominant velocity component and the rock face at
874 PD1 site, however, appears to be less than ~20º and possibly is not as favourable for triggering
875 rockfalls as for other sites. On the other hand, the particle motion hodogram has two dominant
876 directions; WNW and WSW. Depending on the strike of the rock face, either one of these
877 directions can orient particle motion favourably for rockfalls. For instance, site RAP has a rock
878 face strike of 25º, which is sub-parallel to the WSW particle motion direction. However, the
879 WNW particle motion direction makes a steep angle with the rock face and thus can promote
880 rockfalls. Combining information from particle velocity and motion hodograms, we
881 hypothesize that directional aspects were favourable to rockfall triggering at the Rapaki and
882 Purau sites.
883
884 **5.8 Pre-existing rockfalls as predictive database**
885

https://doi.org/10.5194/nhess-2019-178
Preprint. Discussion started: 11 June 2019

Our study indicates that pre-CES rockfalls provide an accurate range of expected boulder volumes, shapes, and % lithologic variance (i.e. VB vs CL), but underestimates expected average and maximum runout distances (on interfluves) because pre-CES rockfalls were probably emplaced on a forested hillslope. Conversely, the final resting locations for pre-CES boulders in well-established drainage valleys/channels may overestimate the expected runout for future rockfalls because the rockfalls have been remobilized after their initial emplacement.

Prior to the CES, rockfall hazard was not considered a high threat in Banks Peninsula and surrounding areas (Townsend and Rosser, 2012), including the Port Hills of southern Christchurch, where damage was most critical and 5 fatalities occurred (Massey et al., 2014). To date, we are aware of only four studies that have dated pre-CES rockfalls in Banks Peninsula (Mackey and Quigley, 2014; Borella et al., 2016b, Sohbati et al., 2016; Litchfield et al., 2016), and all of these investigations occurred after the CES. We assume this was primarily because there were few records of historical rockfall occurrence, and of those described (Lundy, 1995), none hinted at the potential for future widespread cliff collapse and rockfall in the region. However, the geologic record (i.e. prehistoric rockfalls) provides evidence that rockfall events of similar magnitude (or greater) have occurred in the past. In regions devoid of historical or contemporary rockfalls, pre-existing rockfalls represent the only empirical proxy for evaluating local rockfall behavior and provide valuable input for rockfall modeling and risk assessment studies. Existing rockfalls provide valuable data for predicting rockfall volumetric, lithologic, and morphologic (i.e. boulder shape) characteristics, but a thorough consideration of landscape evolutionary chronologies (including deforestation) and post-emplacement mobility scenarios is required before pre-existing rockfalls can be confidently used as future spatial indicators.

6 Conclusions

The spatial distributions and physical-geological properties of individual (n=1093) rockfall boulders deposited at two sites in Banks Peninsula prior to the 2010-2011 Canterbury earthquake sequence (CES) are compared to boulders (n=185) deposited during the CES. Pre-CES to CES boulder ratios range between 5:1 and 8.5:1 respectively, suggesting preservation of multiple pre-CES rockfall events with a flux analogous to or smaller than CES events, and / or pre-CES event(s) of larger flux. Pre-CES and CES boulders at one site (Purau site) have statistically-consistent power-law frequency-volume distributions between 1.0 to >100.0 m^3. At the Rapaki site, CES boulders have smaller and more clustered volumetric distributions that

https://doi.org/10.5194/nhess-2019-178
Preprint. Discussion started: 11 June 2019


Natural Hazards and Earth System Sciences
Discussions

are less well fit by power-laws compared with the pre-CES data, interpreted to reflect variations in rockfall source characteristics through time. Boulders of volcanic breccia (VB) have a larger binned-percentage of large volume boulders and more equant boulder aspects relative to coherent lava (CL) boulder lithologies at both sites, revealing lithologic controls on rockfall physical properties. The maximum runout distances for Rapaki CES VB and CL boulders are greater than that of pre-CES boulders of equivalent lithologies, volumes and morphologies. This is interpreted as an effect of anthropogenic deforestation on the hosting hillslope, which enabled CES boulders to travel further than their pre-CES counterparts due to reduced resistance from vegetation. At Purau, isolated geomorphic domains exhibit this same effect, however in other intra-site locations, pre-CES boulder locations exceed runout distances of CES boulders. This is interpreted to reflect post-depositional mobility of prehistoric boulders via debris flows and other surface processes, reduction of CES boulder runouts in channels due to collisional impedance from pre-CES boulders, and heterogeneity in the CES boulder distributions, which reduced the likelihood of large runout boulders occurring due to smaller volumetric fluxes. The shadow angle method is a reliable predictor for pre-CES and CES rockfall runout at both sites. At Rapaki, the pre-CES and CES rockfall data is best fit using a 2nd order polynomial regression, while at Purau rockfalls require a variety of data fits (e.g. linear, log, polynomial), suggesting intra-site geomorphic and geologic factors affecting rockfall hazard are spatially variable. Bare-earth and forested numerical modeling suggest that the majority of pre-CES rockfalls were emplaced before deforestation of the Purau hillslopes and enables identification of boulder sub-populations that have likely experienced post-emplacement mobility. Our study highlights the challenges of using rockfall distributions to characterize future rockfall hazards in the context of geologic and geomorphic variations, including natural and anthropogenically-influenced landscape changes.

Acknowledgements. Financial support for the project came from the EQC (Earthquake Commission) capability fund for South Island geohazards research. J.B. thanks Sarah Trutner, Peter Borella, Maxwell Borella, Peter Almond, Simon Brocklehurst, David Bell, and Jarg Pettinga. Special thanks to Pip and David Barker for allowing us land access in Purau and review of the Camp Bay geotechnical property report. The authors declare that they have no competing interests.

https://doi.org/10.5194/nhess-2019-178
Preprint. Discussion started: 11 June 2019

Natural Hazards and Earth System Sciences
Discussions

References

Agliardi, F. and Crosta, G. B.: High resolution three-dimensional numerical modeling of rockfalls, Int. J. Rock Mech. Min. Sci., 40, 455–471, 2003, doi:10.1016/S1365-1609(03)00021-2.

Geotechnical Report prepared for Purau Properties Ltd. by Eliot Sinclair and Partners Ltd., Camp Bay Road, Purau, 18 pp., 2011.

Bartelt, P., Buehler, Y., Christen, M., Deubelbeiss, Y., Graf, C., and McArdell, B. W.: RAMMS - rapid mass movements simulation: A numerical model for rockfall in research practice, User Manual v1.5. Davos, Switzerland, 102 pp., 2013.

Bell, D. H. and Trangmar, B. B.: Regolith materials and erosion processes on the Port Hills, Christchurch, New Zealand, Fifth International Symposium on Landslides, Lausanne: A. A. Balkema, 93-105, 1987.

Borella J., Quigley M., and Vick, L.: Anthropocene rockfalls travel farther than prehistoric predecessors, Sci. Adv., 2, e1600969, 2016.

Borella, J., Quigley, M., Sohbati, R., Almond, P., Gravley, D.M., and Murray, A.: Chronology and processes of late Quaternary hillslope sedimentation in the eastern South Island, New Zealand, J. Quat. Sci., 31, 691-712, 2016, doi: 10.1002/jqs.2905.

Bouchon, M. and Barker, J. S.: Seismic response of a hill: The example of Tarzana, California, Seismol. Soc. Am. Bull., 86(1A), 66 – 72, 1996.

Bradley, B. A., and Cubrinovski, M.: Near-source strong ground motions observed in the 22 February 2011 Christchurch earthquake. Seismol. Res. Lett., 82, 853 – 865, 2011. https://doi.org/10.1785/gssrl.82.6.853

Bradley, B. A.: Ground motions observed in the Darfield and Christchurch earthquakes and the importance of local site response effects, New Zealand Journal of Geology and Geophysics, 55(3), 279 – 286, 2012. https://doi.org/10.1080/00288306.2012.674049

Bradley, B. A.: Strong ground motion characteristics observed in the 13 June 2011 Mw6.0 Christchurch, New Zealand earthquake, Soil Dynamics and Earthquake Engineering, 91, 23 – 38, 2016. http://dx.doi.org/10.1016/j.soildyn.2016.09.006

Burjánek, J., Gischig, V., Moore, J. R. and Fäh, D.: Ambient vibration characterization and monitoring of a rock slope close to collapse, Geophys. J. Int., 212, 297 – 310, 2018. https://doi.org/10.1093/gji/ggx424

Carey, J. M., Misra, S., Bruce, Z. R., and Barker, P. R.: Canterbury Earthquakes 2010/11 Port Hills Slope Stability: Laboratory Testing Factual Report, GNS Science Consultancy Report 2014/53, GNS Science, Lower Hutt, 88 pp., 2014.

Christensen, N. I., Wilkens, R. H. and Blair, S. C.: Seismic velocities, densities, and elastic constants of volcanic breccia and basalts from deep sea drilling project leg 59, Initial Reports of the Deep Sea Drilling Project, LIX, Washington, pp. 515 – 517, 1980.

https://doi.org/10.5194/nhess-2019-178
Preprint. Discussion started: 11 June 2019

Natural Hazards and Earth System Sciences
Discussions

Copons, R. and Vilaplana, J. M.: Rockfall susceptibility zoning at a large scale: From geomorphological inventory to preliminary land use planning, Eng. Geol., 102, 142–151, 2008.

Copons, R., Vilaplana, J. M., and Linares, R.: Rockfall travel distance analysis by using empirical models (Sola d'Andorra la Vella, Central Pyrenees), Nat. Hazards Earth Syst. Sci. 9, 2107–2118, 2009.

Dorren, L.: A review of rockfall mechanics and modelling approaches, Prog. Phys. Geog., 27(1), 69–87, 2003.

Dorren, L., Maier, B., Putters, U. S., and Seijmonsbergen, A. C.: Combining field and modelling techniques to assess rockfall dynamics on a protection forest hillslope in the European Alps, Geomorphology, 57, 151-167, 2004, doi:10.1016/S0169-555X(03)00100-4.

Dussauge-Peisser, C., Helmstetter, A., Grasso, J.-R., Hantz, D., Desvarreux, P., Jeannin, M., and Giraud, A.: Probabilistic approach to rock fall hazard assessment: potential of historical data analysis, Nat. Hazards Earth Syst. Sci., 2, 15–26, 2002, http://www.nat-hazards-earth-syst-sci.net/2/15/2002/.

Evans, S. G. and Hungr, O.: The assessment of rockfall hazard at the base of talus slopes, Can. Geotech. J., 30, 620–636, 1993.

Guzzetti, F., Malamud, B. D., Turcotte, D. L., and Reichenbach, P.: Power-law correlations of landslide areas in central Italy, Earth Planet. Sci. Lett., 195, 169-183, 2002.

Guzzetti, F., Reichenbach, P., and Wieczorek, G. F.: Rockfall hazard and risk assessment in the Yosemite Valley, California, USA, Nat. Hazards Earth Syst. Sci., 3, 491–503, 2003, http://www.nat-hazards-earth-syst-sci.net/3/491/2003/.

Guzzetti, F., Reichenbach, P., and Ghigi, S.: Rockfall hazard and risk assessment along a transportation corridor in the Nera Valley, Central Italy, Environ. Manage., 34, 191-208, 2004, doi:10.1007/s00267-003-0021-6.

Hampton, S.J. and Cole, J.W.: Lyttelton Volcano, Banks Peninsula, New Zealand: Primary volcanic landforms and eruptive centre identification, Geomorphology, 104, 284-298, 2009, doi:10.1016/j.geomorph.2008.09.005.

Hartzell, S. H., Carver, D. L. and King, K. W.: Initial investigation of site and topographic effects, at Robinwood Ridge, Bull. Seismol. Soc. Am., 84(5), 1336 – 1349, 1994.

Heron, D., Lukovic, B., Massey, C., Ries, W., and McSaveney, M.: GIS modelling in support of earthquake-induced rockfall and cliff collapse risk assessment in the Port Hills, Christchurch. J. Spat. Sci. 59, 313-332, 2014, doi: 10.1080/14498596.2014.913509.

Kaiser, A. E., Holden, C. and Massey, C. I.: Site amplification, polarity and topographic effects in the Port Hills during the Canterbury earthquake sequence, GNS Science Consultancy Report 2014/121, 33 p., 2014.

https://doi.org/10.5194/nhess-2019-178
Preprint. Discussion started: 11 June 2019

1052 Keefer, D.K.: Landslides caused by earthquakes. Geol. Soc. Am. Bull. 95, 406-421, 1984.
1053
1054 Kleinbrod, U., Burjánek, J., and Fäh, D.: On the seismic response of instable rock slopes
1055 based on ambient vibration recordings, Earth Planets Space, 69, 126, pp. 9, 2017.
1056 doi:10.1186/s40623-017-0712-5. https://doi.org/10.1186/s40623-017-0712-5
1057
1058 Lan, H., Martin, C. D., Zhou, C., and Lim, C. H.: Rockfall hazard analysis using LiDAR and
1059 spatial modeling, Geomorphology, 118, 213-223, 2010,
1060 doi:10.1016/j.geomorph.2010.01.002.
1061
1062 Latham, J-P., Munjiza, A., Garcia, X., Xiang, J., and Guises, R.: Three-dimensional particle
1063 shape acquisition and use of shape library for DEM and FEM/DEM simulation, Min. Eng.,
1064 21, 797-805, 2008, doi:10.1016/j.mineng.2008.05.015.
1065
1066 Lee, S-J.: Lessons learned from source rupture to strong ground motion simulations: An
1067 example from Taiwan, Bull. Seismol. Soc. Am., 107(5), 2106 – 2116, 2017.
1068 https://doi.org/10.1785/0120170030
1069
1070 Leine, R.I., Schweizer, A., Christen, M., Glover, J., Bartelt, P., and Gerber, W.: Simulation of
1071 rockfall trajectories with consideration of rock shape, Multibody Syst. Dyn., 32, 241-271,
1072 2013, doi:10.1007/s11044-013-9393-4.
1073
1074 Lied, K.: Rockfall problems in Norway, in: Rockfall dynamics and protective work
1075 effectiveness, Instituto Sperimentale Modelli e Structture (ISMES), Bergamo, Italy, 90, 51–
1076 53, 1977.
1077
1078 Litchfield, N. J., Van Dissen, R. J., Massey, C. I.: Pre-Christchurch earthquake sequence
1079 rockfalls in the Port Hills, Christchurch: Wakefield Avenue Trench, GNS Science
1080 Consultancy Report 2016/25, GNS Science, Lower Hutt, 32 pp., 2016.
1081
1082 Mackey, B.H. and Quigley, M.C.: Strong proximal earthquakes revealed by cosmogenic ^{3}He
1083 dating of prehistoric rockfalls, Christchurch, New Zealand. Geology 42, 975–978, 2014.
1084
1085 Massey, C. I., Gerstenberger, M., McVerry, G., and Litchfield, N.: Canterbury earthquakes
1086 2010/11 Port Hills slope stability: additional assessment of the life-safety risk from rockfalls
1087 (boulder rolls). GNS Science Consultancy Report 2012/214, GNS Science, Lower Hutt, pp.
1088 18, 2012a,
1089 http://resources.ccc.govt.nz/files/Homeliving/civildefence/chchearthquake/gns_ph_additional
1090 assessmtrockfalls12687628.pdf
1091
1092 Massey, C. I., McSaveney, M. J., Heron, D., and Lukovic, B.: Canterbury earthquakes
1093 2010/11 Port Hills slope stability: pilot study for assessing life-safety risk from rockfalls
1094 (boulder rolls). GNS Science Consultancy Report 2011/311, GNS Science, Lower Hutt, pp.
1095 74, 2012b,
1096 http://resources.ccc.govt.nz/files/Homeliving/civildefence/chchearthquake/porthills/CR2011-
1097 311-01AUG2013.pdf
1098
1099 Massey, C. I., McSaveney, M. J., Yetton, M. D., Heron, D., Lukovic, B., and Bruce, Z. R. V.:
1100 Canterbury earthquakes 2010/11 Port Hills slope stability: pilot study for assessing life-safety
1101 risk from cliff collapse. GNS Science Consultancy Report 2012/57, GNS Science, Lower

https://doi.org/10.5194/nhess-2019-178
Preprint. Discussion started: 11 June 2019

Hutt, pp. 101, 2012c, http://resources.ccc.govt.nz/files/Homeliving/civildefence/chchearthquake/gns_ph_pilotlifesafetycliffcollapse12687374web.pdf

Massey, C. I., McSaveney, M. J., Lukovic, B., Heron, D., Ries, W., Moore, A., and Carey, J.: Canterbury earthquakes 2010/11 Port Hills slope stability: life-safety risk from rockfalls (boulder rolls). GNS Science Consultancy Report 2012/123. GNS Science, Lower Hutt, pp. 34, 2012d, http://resources.ccc.govt.nz/files/Homeliving/civildefence/chchearthquake/gns_ph_lifesafetyrockfall12684517web-s.pdf.

Massey, C. I., McSaveney, M. J., and Heron, D.: Canterbury earthquakes 2010/11 Port Hills slope stability: life-safety risk from cliff collapse in the Port Hills, GNS Science Consultancy Report 2012/124, GNS Science, Lower Hutt, pp 35., 2012e, http://resources.ccc.govt.nz/files/Homeliving/civildefence/chchearthquake/gns_ph_lifesafetycliffcollapse12684515web-s.pdf

Massey, C. I., Yetton, M. J., Carey, J., Lukovic, B., Litchfield, N., Ries, W., and McVerry, G.: Canterbury earthquakes 2010/11 Port Hills slope stability: stage 1 report on the findings from investigations into areas of significant ground damage (mass movements), GNS Science Consultancy Report 2013/317, GNS Science, Lower Hutt, pp. 37, 2013, http://resources.ccc.govt.nz/files/Homeliving/civildefence/chchearthquake/porthills/CR2012-317Stage1.pdf

Massey, C. I., McSaveney, M. J., Taig, T., Richards, L., Litchfield, N. J., Rhoades, D. A., McVerry, G. H., Lukovic, B., Heron, D. W., Ries, W., and Van Dissen, R. J.: Determining rockfall risk in Christchurch using rockfalls triggered by the 2010-2011 Canterbury earthquake sequence, Earthquake Spectra, 30, 155-181, 2014, DOI: 10.1193/021413EQS026M.

Massey, C., Della Pasqua, F., Holden, C., Kaiser, A., Richards, L., Wartman, J., McSaveney, M. J., Archibald, G., Yetton, M., and Janku, L.: Rock slope response to strong earthquake shaking. Landslides 14, 249-268, 2017, doi:10.1007/s10346-016-0684-8.

Muktar, J-A. S.: Engineering geological and geotechnical characterization of selected Port Hills lavas, Master's thesis, Department of Geological Sciences, University of Canterbury, New Zealand, pp. 172, 2014.

Porter, S. C. and Orombelli, G.: Alpine rockfall hazards: Recognition and dating of rockfall deposits in the western Italian Alps lead to an understanding of the potential hazards of giant rockfalls in mountainous regions, Am. Sci., 69, 67-75, 1981, https://www.jstor.org/stable/27850249.

Quigley M. C., Hughes, M. W., Bradley, B. A., van Ballegooy, S., Reid, C., Morgenroth, J., Horton, T., Duffy, B., and Pettinga, J. R.: The 2010-2011 Canterbury Earthquake Sequence: Environmental effects, seismic triggering thresholds and geological legacy, Tectonophysics, 672-673, 228-274, 2016.

Sewell, R.J.: Late Miocene volcanic stratigraphy of central Banks Peninsula, Canterbury, New Zealand, New Zeal. J. Geol. Geop., 31, 41-64, 1988,

https://doi.org/10.5194/nhess-2019-178
Preprint. Discussion started: 11 June 2019

Natural Hazards and Earth System Sciences
Discussions

doi:10.1080/00288306.1988.10417809.

Sohbati, R., Borella, J., Murray, A., Quigley, M., Buylaert, J.: Optical dating of loessic hillslope sediments constrains timing of prehistoric rockfalls, Christchurch, New Zealand. Journal of Quaternary Science, 31, 678-690, 2016, doi: 10.1002/jqs.2895.

Spetzler, J. and Snieder, R.: The Fresnel volume and transmitted waves, Geophysics, 69(3), 653 – 663, 2004. https://doi.org/10.1190/1.1759451

Stock, G. M., Luco, N., Collins, B. D., Harp, E. L., Reichenbach, P., Frankel, K. L.: Quantitative rock-fall hazard and risk assessment for Yosemite Valley, Yosemite National Park, California: U.S. Geological Survey Scientific Investigations Report 2014-5129, 52 p., 2014.

Takemura, S., Furumura, T. and Maeda, T.: Scattering of high-frequency seismic waves caused by irregular surface topography and small-scale velocity inhomogeneity, Geophys. J. Inter., 201(1), 459–474, 2015. https://doi.org/10.1093/gji/ggv038

Townsend, D. B., Rosser, B.: Canterbury earthquakes 2010/2011 Port Hills slope stability: Geomorphology mapping for rockfall risk assessment, GNS Science Consultancy Report 2012/15, GNS Science, Lower Hutt, pp. 21, 2012.

Van Houtte, C., Ktenidou, O.-J., Larkin, T., and Kaiser, A.: Reference stations for Christchurch, Bulletin of the New Zealand Society for Earthquake Engineering, 45(4), 184 – 195, 2012.

Varnes, D. J.: Slope movement types and processes, in: Landslides: analysis and control, edited by: Schuster, R. L. and Krizek, R. L., Transportation Research Board, National Research Council, Washington, special report 176, 11–33, 1978.

Vick, L.M., Zimmer, V., White, C., Massey, C., and Davies, T.: Significance of substrate soil moisture content for rockfall hazard assessment. Nat. Hazards Earth Syst. Sci. 19, 1105-1117, 2019.

Vick, L.M.: Evaluation of field data and 3D modelling for rockfall hazard assessment, Ph.D. thesis, Department of Geological Sciences, University of Canterbury, New Zealand, pp. 173, 2015.

Wieczorek, G. F.: Catastrophic rockfalls and rockslides in the Sierra Nevada, USA. Geol. Soc. Am. Rev Eng. Geol., 15, 1-26, 2002.

Wieczorek, G. F., Stock, G. M., Reichenbach, P., Snyder, J. B., Borchers, J.W., and Godt, J.W.: Investigation and hazard assessment of the 2003 and 2007 Staircase Falls rock falls, Yosemite National Park, California, USA, Nat. Hazards Earth Syst. Sci., 8, 421–432, 2008, http://www.nat-hazards-earth-syst-sci.net/8/421/2008/.

	Rapaki Pre-CES (n=409)	*Rapaki CES (n=48)*	*Difference*	*Difference*	*Purau Pre-CES (n=684)*	*Purau CES (n=136)*	*Difference*	*Difference*
	(m^3)	(m^3)	(m^3)	(%)	(m^3)	(m^3)	(m^3)	(%)
25th (Q1)	1.60	1.36	0.24	17.65	1.42	1.34	0.08	5.97
Median	2.94	2.21	0.73	33.03	2.20	2.01	0.19	9.45
75th (Q3)	6.59	4.83	1.76	36.44	5.08	4.46	0.62	13.90
95th	20.54	19.76	0.78	3.95	27.06	17.66	9.4	53.23
Maximum	200.56	28.35	172.21	607.44	616.00	79.97	536.03	670.29
Mean	6.81	4.84	1.97	40.70	8.10	5.32	2.78	52.26

Table 1. Volumetric comparison of pre-CES and CES rockfall boulders (for volume ≥1.0 m^3) at Rapaki and Purau study sites.

	Rapaki				***Purau***			
	Pre-CES	CES	Pre-CES	CES	Pre-CES	CES	Pre-CES	CES
	VB (n=391) (m^3)	VB (n=45) (m^3)	CL (n=18) (m^3)	CL (n=3) (m^3)	VB (n=436) (m^3)	VB (n=127) (m^3)	CL (n=248) (m^3)	CL (n=9) (m^3)
25th (Q1)	1.68	1.39	1.22	1.03	1.70	1.36	1.20	1.13
Median	3.1	2.21	1.38	1.06	3.21	2.04	1.56	1.68
75th (Q3)	6.78	5.7	1.54	1.67	7.65	4.87	2.30	2.14
95th	21.28	20.576	3.92	2.16	40.91	17.78	5.26	2.48
Maximum	200.56	28.35	9.99	2.28	616.00	79.97	26.21	2.64
Mean	7.03	5.06	1.96	1.45	11.43	5.58	2.24	1.67
Total volume	2749.07	227.80	35.29	4.34	4938.76	708.34	555.63	15.00
% of total volume	99	98	1	2	89	98	11	2
% of mapped boulders	96	94	4	6	64	93	36	7

Table 2. Comparison of boulder size statistics for Rapaki and Purau VB and CL pre-CES and CES rockfall boulders (volume ≥1.0 m^3).

	# of pre-CES rockfalls : # of CES rockfalls	*pre-CES : CES*	*pre-CES : CES*	*volume of pre-CES rockfalls: volume of CES rockfalls*	*pre-CES : CES*	*pre-CES : CES*
	(n)	ratio	% : %	(m^3)	ratio	% : %
Total (Rapaki + Purau)	1093 : 184	5.94	86 : 14	8323.76 : 955.48	8.71	90 : 10
Rapaki Total	409 : 48	8.52	89 : 11	2784.37 : 232.14	11.99	92 : 8
Rapaki VB	391 : 45	8.69	90 : 10	2749.07 : 227.80	12.07	92 : 8
Rapaki CL	18 : 3	6.00	86 : 14	35.29 : 4.34	8.14	89 : 11
Purau Total	684 : 136	5.03	83 : 17	5539.39 : 723.35	7.66	88 : 12
Purau VB	436 : 127	3.43	77 : 23	4983.76 : 708.34	7.04	88 : 12
Purau CL	248 : 9	27.56	96 : 4	555.63 : 15.00	37.04	97 : 3

Table 3A. Comparison of frequency (n) and volume (m^3) ratios for pre-CES and CES rockfall boulders at the Rapaki and Purau study sites.

	# of VB boulders : # of CL boulders	*VB : CL*	*VB : CL*	*Volume of VB boulders : volume of CL boulders*	*VB:CL*	*VB:CL*
	n : n	ratio	% : %	m^3 : m^3	ratio	% : %
Total (Rap + Purau)	999 : 278	3.59	78 : 22	8668.97 : 610.26	14.21	93 : 7
Rapaki Total (pre-CES + CES)	436 : 21	20.76	95: 5	2976.87 : 39.63	75.11	99 : 1
Rapaki pre-CES	391 : 18	21.72	96 : 4	2749.07 : 35.29	77.9	99 : 1
Rapaki CES	45 : 3	15	94 :6	227.80 : 4.34	52.49	98 : 2
Purau Total (pre-CES + CES)	563 : 257	2.19	69 : 31	5692.1 : 570.63	9.98	91 : 9
Purau pre-CES	436 : 248	1.76	64 : 36	4983.76 : 555.63	8.97	90 : 10
Purau CES	127 : 9	14	93 : 7	708.34 : 15.00	47.22	98 : 2
Purau D1 pre-CES	17 : 0	N/A	100 : 0	137.27 : 0	N/A	100 : 0
Purau D1 CES	30 : 0	N/A	100 : 0	125.86 : 0	N/A	100 : 0
Purau D2 pre-CES	36 : 3	12	92 : 8	230.8 : 3.9	59.18	98 : 2
Purau D2 CES	1 : 1	1	50 : 50	14.78 : 1.08	13.69	93 : 7
Purau D3 pre-CES	54 : 43	1.26	56 : 44	203.79 : 142.62	1.43	59 : 41
Purau D3 CES	38 : 3	12.67	93 : 7	242.63 : 5.91	41.05	98 : 2
Purau D4 pre-CES	8 : 1	8	89 : 11	188.42 : 1.24	151.95	99 : 1
Purau D4 CES	36 : 0	N/A	100 : 0	267.76 : 0	N/A	100 : 0

Table 3B. Comparison of VB/CL frequency (n) and volume (m^3) ratios for pre-CES and CES rockfall boulders at the Rapaki and Purau study sites.

https://doi.org/10.5194/nhess-2019-178
Preprint. Discussion started: 11 June 2019

Natural Hazards and Earth System Sciences
Discussions

Runout Distance (MLR)	*Average* (m)	*Maximum* (m)
Rapaki		
Pre-CES	184.30	567.51
CES	276.23	702.47
Pre-CES VB	*184.65*	*567.51*
Pre-CES CL	*176.57*	*346.73*
CES VB	*276.91*	*702.47*
CES CL	*266.13*	*432.14*
Purau		
PD1 Pre-CES	29.86	96.96
PD1 CES	119.63	348.4
PD2 Pre-CES	84.01	279.75
PD2 CES	14.11	15.91
PD3 Pre-CES	239.62	462.8
PD3 CES	237.24	413.35
PD4 Pre-CES	109.11	208.85
PD4 CES	181.75	304.56
PD1 Pre-CES VB	29.86	96.96
PD1 CES VB	119.63	348.4
PD1 Pre-CES CL	*N/A*	*N/A*
PD1 CES CL	*N/A*	*N/A*
PD2 Pre-CES VB	*88.73*	*279.75*
PD2 CES VB	*12.3*	*12.3*
PD2 Pre-CES CL	*27.39*	*33.38*
PD2 CES CL	*15.91*	*15.91*
PD3 Pre-CES VB	*248.96*	*434.85*
PD3 CES VB	*243.21*	*413.35*
PD3 Pre-CES CL	*227.89*	*462.8*
PD3 CES CL	*161.68*	*178.53*
PD4 Pre-CES VB	*106.99*	*208.85*
PD4 CES VB	181.75	304.56
PD4 Pre-CES CL	*126.06*	*126.06*
PD4 CES CL	*N/A*	*N/A*

MLR = Map Length Runout
PD1 = Purau Domain 1

Table 4. Average and maximum runout distances for pre-CES and CES rockfall boulders (for volume ≥1.0 m^3) at Rapaki and Purau study sites.

https://doi.org/10.5194/nhess-2019-178
Preprint. Discussion started: 11 June 2019

Natural Hazards and Earth System Sciences
Discussions

Figure Captions

Fig. 1. **(A)** Google Earth image showing Rapaki and Purau study sites. CES rockfall locations as mapped by GNS Science and the author (at Rapaki and Purau) are shown (red). Epicenter locations for 22 February, 13 June, and 16 April 2011 events are displayed [Modified from Massey et al. (2014)]. Inset map of South Island (New Zealand) shows Banks Peninsula and approximate location for study site (yellow star). **(B)** Anthropogenic deforestation of Banks Peninsula. Removal of native forest occurred rapidly in Banks Peninsula (BP) with arrival of Polynesians (c. AD 1280) then Europeans (c. AD 1830). Before Polynesian (Maori) arrival, extensive native forest was present throughout BP. Prior to European settlement, minor to moderate removal of indigenous forest by Maori occurred, with burning being the primary tool for clearance (yellow). By 1920 Europeans had removed >98% of BP native forest (red). Minor re-establishment of old-growth native forest has occurred (green) but slopes in the Port Hills and greater BP (including Rapaki and Purau) remain largely unvegetated.

Fig. 2. **(A)** Mapped pre-CES volcanic breccia (VB) and coherent lava (CL) boulders at Rapaki. The largest boulders with the furthest runout distances are comprised exclusively of volcanic breccia. Ratio of pre-CES VB to CL boulders is ~22:1. **(B)** Mapped CES VB and CL boulders at Rapaki study site. Note the low number of CL rockfall boulders detached during the CES at Rapaki. Ratio of CES VB to CL boulders is 15:1. [a = volcanic source rock; b = dominated by volcanic boulder colluvium and volcanic loess colluvium; c = loess-colluvium underlain by in-situ loess and volcanic rock; d = alluvial sediments overlying loess and bedrock]

Fig. 3. **(A)** Mapped pre-CES and CES rockfalls with volume ≥1.0 m^3 at Purau study site. Ratio of pre-CES to CES boulders is ~5:1. A= volcanic source rock; B=dominated by volcanic boulder colluvium and volcanic loess colluvium; C=loess-colluvium underlain by in-situ loess and volcanic rock; D=alluvial sediments overlying loess and bedrock. **(B)** Mapped pre-CES VB and CL boulders at Purau. Ratio of pre-CES VB to CL boulders is ~2:1. **(C)** Mapped CES VB and CL boulders at Purau study site. Note the low number of CL rockfall boulders detached during the CES at Purau. Ratio of CES VB to CL boulders is ~14:1. PD1-PD4 represent Purau rockfall domains.

Fig. 4. Pre-CES and CES VB boulders at Rapaki and Purau study sites. **(A)** Pre-CES boulder in footslope position with smaller CES boulder at right bottom. **(B)** Exploratory trenching exposes the colluvial sediment wedge at the boulder backside depicted in Fig. 7B. **(C)** Pre-CES boulder at Purau study site. Erosion of the surrounding hillslope sediments has exposed the boulder base and underlying loessic sediment. **(D)** Advanced surface roughness and abundant lichen growth on pre-CES boulder surface. **(E)** Large CES boulder (~28 m^3) detached from Mount Rapaki and emplaced in the Rapaki village during the 22 February 2011 earthquake (photo courtesy of D.J.A. Barrell, GNS Science). **(F)** CES boulder showing 2011 detachment surface [1] and adjacent non-detached surface [2] with higher degree of rough. **(G-K)** Representative CL boulders at Rapaki and Purau sites exhibit typical elongate and flat morphologies.

Fig. 5. **(A)** Volcanic source rock at Rapaki study site. Sixty (60) individual detachment zones were created during the CES (yellow) and represent ~9% of the total source rock area. The source rock is comprised of ~86% VB and ~14% CL. ~69% and ~31% of the detachments occurred within the VB and CL lithologies, respectively. **(B)** Photo showing

https://doi.org/10.5194/nhess-2019-178
Preprint. Discussion started: 11 June 2019

Natural Hazards and Earth System Sciences
Discussions

several irregularly shaped CES detachment zones near the top of Mt. Rapaki. **(C)** Photo showing freshly exposed VB and CL layering within the Rapaki source rock. **(D)** Portion of volcanic source rock at Purau showing VB and CL layering. A single CES detachment site is shown at the top of the source rock. Seven (7) individual CES detachment sites were identified at the Purau study site. **(E)** CL and VB layers at the Purau study site. Note the thickness of the CL layer (~5-7 meters) and lack of any CES detachment sites despite the high degree of fracturing and overhanging condition. **(F)** VB and CL layering in Sumner (Christchurch) cliff exposure adjacent to Main Road. Extensive cliff collapse during the CES has revealed multiple lava flows and the distinctive textural differences between the VB and CL lithologies. Note the high density of vertical to subvertical fractures within the CL layers. **(G)** Exposed lava layers adjacent to Main Road in Redcliffs (Christchurch). Note the single-family living residence at top of photo.

Fig. 6. Relative locations of stations LPCC, D13C, D15C, and GODS (yellow squares). Also shown are epicentres of 2011-02-21 Mw 6.2 and 2011-06-13 Mw 6 earthquakes (yellow stars) along with Rapaki and Purau sites.

Fig. 7. Each panel shows seismic data from LPCC (A and B), D13C (C), D15C (D), and GODS (E) stations. Panels A and B compare ground motion, respectively, for 2011-02-21 Mw 6.2 and 2011-06-13 Mw 6 earthquakes at LPCC station. The left column shows east and north components of the velocity seismogram (blue line) and their respective envelopes (red dashed-line). The particle velocity hodogram (middle column, green line) was determined for a time window ± 5 s (shaded region in the left column) around the peak (red circle) of the east component envelope. The strike of the rock face (black short line segments) and the direction of the free face (red arrows) for sites PD1, PD2, PD3, PD4, and RAP are also illustrated. The particle motion hodogram (grey line) is presented in the right column, where green, yellow, and red segments represent, respectively, time points at which east component, north component, or both components exceed an acceleration of 0.3g. Note that scale of figure axes varies by station particularly for ground motion.

Fig. 8. **(A)** Rockfall size distribution as a proportion of boulders less than a given size plotted in log-space for CES and pre-CES rockfalls at Rapaki. **(B)** Rockfall frequency/size distribution for CES and pre-CES rockfalls at Rapaki. **(C)** Rockfall size distribution as a proportion of boulders less than a given size plotted in log-space for CES and pre-CES rockfalls at Purau. **(D)** Rockfall frequency/size distribution for CES and pre-CES rockfalls at Purau. **(E)** Comparison of boulder size distributions for CES and pre-CES VB and CL rockfalls at Rapaki study site. **(F)** Comparison of boulder size distributions for CES and pre-CES VB and CL rockfalls at Purau.

Fig. 9. **(A)** Frequency ratio versus volume ratio for pre-CES and CES rockfall boulders. **(B)** Frequency-runout distributions for Rapaki pre-CES and CES boulders. Both power law (without extrapolated data) and exponential fits (all data) are shown for the prehistoric boulder data set. A poor exponential fit is shown for CES rockfalls. **(C)** Plot of travel distance on talus slope (Lt) versus height on talus slope (Ht) with fitted polynomial regression lines for pre-CES and CES rockfalls at Rapaki. **(D)** Plot of Lt versus Ht with fitted linear, log, and polynomial regression lines for pre-CES and CES rockfalls at Purau. Four (4) separated domains (here D1-D4) are defined at Purau to evaluate the shadow angle method. **(E)** Plot of rockfall size (m^3) versus tangent of the shadow angle (Ht/Lt) for Rapaki rockfalls. No tendency of the data is evident. **(F)** Plot of rockfall size (m^3) versus tangent of the shadow

https://doi.org/10.5194/nhess-2019-178
Preprint. Discussion started: 11 June 2019

Natural Hazards and Earth System Sciences
Discussions

angle (Ht/Lt) for Purau rockfalls. The tendency for the domain data sets is poor. Values of correlation coefficients are below 0.3.

Fig. 10. **(A)** RAMMS_1 shows deposited rocks for simulated CES boulders. Mapped CES boulders (red circles; n=136) are shown for comparison. Boulder densities of 2500 kg/m^3 and 3000 kg/m^3 are used for VB and CL boulders, respectively. **(B)** Final resting locations for RAMMS_2 rockfalls. RAMMS-2 assumes prehistoric rockfall conditions (i.e. forested hillslope). Mapped prehistoric rockfalls are depicted (yellow circles) for comparison. An increase in forest density to 10,000 kg/s generates the best fit with maximum runout distance (see white dashed line) for mapped prehistoric boulders. **(C)** Final resting locations for RAMMS_3 boulders. RAMMS_3 assumes modern hillslope conditions (i.e. deforested hillslope) and simulates the future potential rockfall hazard at Purau. The modelling indicates that the distribution of future rockfalls could be widespread and more impactful to existing and proposed development than experienced during the CES. Note the increased maximum runout distance for RAMMS_3 boulders compared with RAMMS_2 and the potential future rockfall hazard to development sites S1 and S2.

Fig. 11. RAMMS simulated rockfall boulders showing differences in spatial distribution between VB (mostly equant shaped) and CL (predominantly elongate and flat shaped) boulder morphologies at Purau. All simulated boulders assume a volume of 1.0 m^3. **(A)** Spatial distribution of simulated VB boulders at Purau CES-7 location. Note the high relative percentage of simulated boulders deposited at the base of the hillslope (~500-600 meters from source rock). **(B)** Spatial distribution of simulated CL boulders at CES-7 location. Note the higher relative percentage of rockfall boulders deposited near the source rock (within ~100 meters from source rock). The simulation highlights the strong influence of boulder shape on runout distance.

Fig. 12. CES and pre-CES rockfall boulders within drainage valleys at Rapaki **(A, C)** and Purau **(B, D, E, F)** study locations. Drainage valleys contain a high amount of pre-CES rockfall boulders, which impacts the trajectory/path of CES rockfalls and stops or reduces runout distance.

Fig. 13. Velocity spectra for the 2011-06-13 Mw 6 earthquake recorded at station D13C. No path corrections are applied.

https://doi.org/10.5194/nhess-2019-178
Preprint. Discussion started: 11 June 2019

Natural Hazards and Earth System Sciences
Discussions

Appendix 1 - Captions

Fig. A1. The total number of boulders with volume ≥ 0.1 m^3 were taken at runout distances of 1-10 m (yellow polygon 1), 30-40 m (yellow polygon 2), 60-70 m (yellow polygon 3), and 100-110 m (yellow polygon 4) from the volcanic source rock to estimate the total number of boulders in areas near the source cliff where conditions were unsafe for continuous mapping. The number of boulders in areas 'b' and 'c' were reduced by factors of 2 and 3, respectively, based upon field observations. The total number of rockfalls boulders for the area (yellow dashed line) was normalized to boulder size of 1.0 m^3 using a power law frequency-size distribution (as determined at the Rapaki study location).

Fig. A2. Conceptual diagram of hillslope illustrating the source rock cliff and the talus slope. The reach angle (A) and shadow angle (B) are shown. Sketch modified from Hungr (1993), Wieczorek et al. (2008) and Copons et al. (2009).

Fig. A3. Final resting locations for RAMMS_2 rockfalls assuming uniform forest density increase of 10,000 kg/s.

Appendix 2 - Captions

Table A1. Friction parameters chosen for each terrain type in RAMMS.

Fig. A1. Polygon shapefiles for runout terrain types.

Fig. A2. Polyline shapefiles for RAMMS_1 rockfall source areas.

Fig. A3. Polyline shapefiles for RAMMS_2 and RAMMS_3 rockfall source areas.

Fig. A4 Polygon shapefiles for forest density.

https://doi.org/10.5194/nhess-2019-178
Preprint. Discussion started: 11 June 2019

Natural Hazards and Earth System Sciences
Discussions
Open Access
EGU

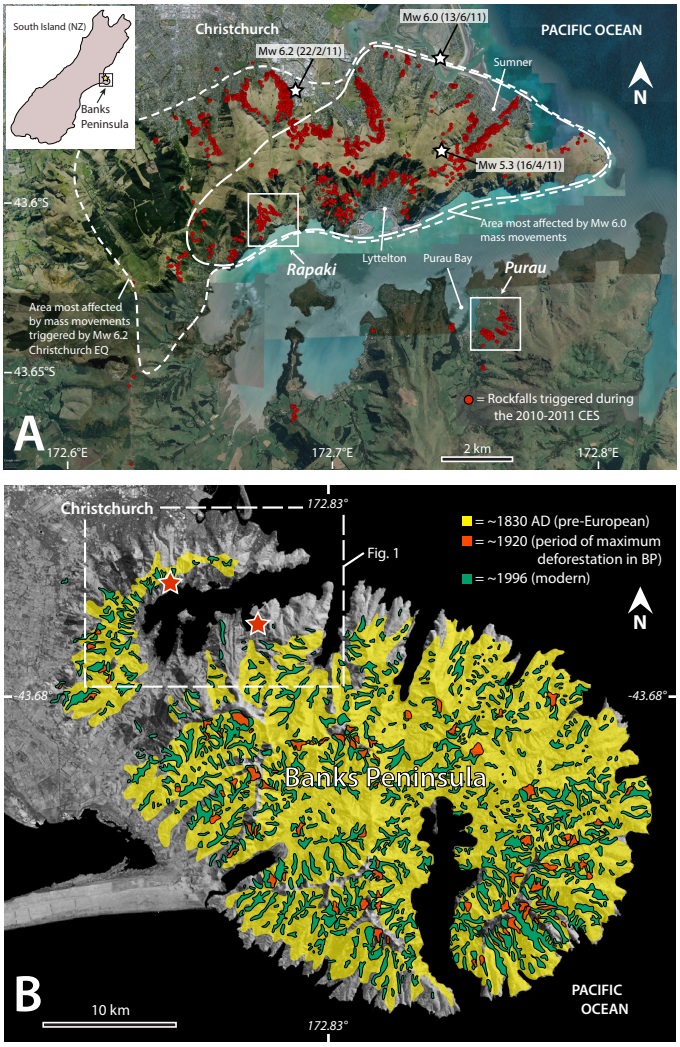

Figure 1

https://doi.org/10.5194/nhess-2019-178
Preprint. Discussion started: 11 June 2019

Natural Hazards and Earth System Sciences
Discussions

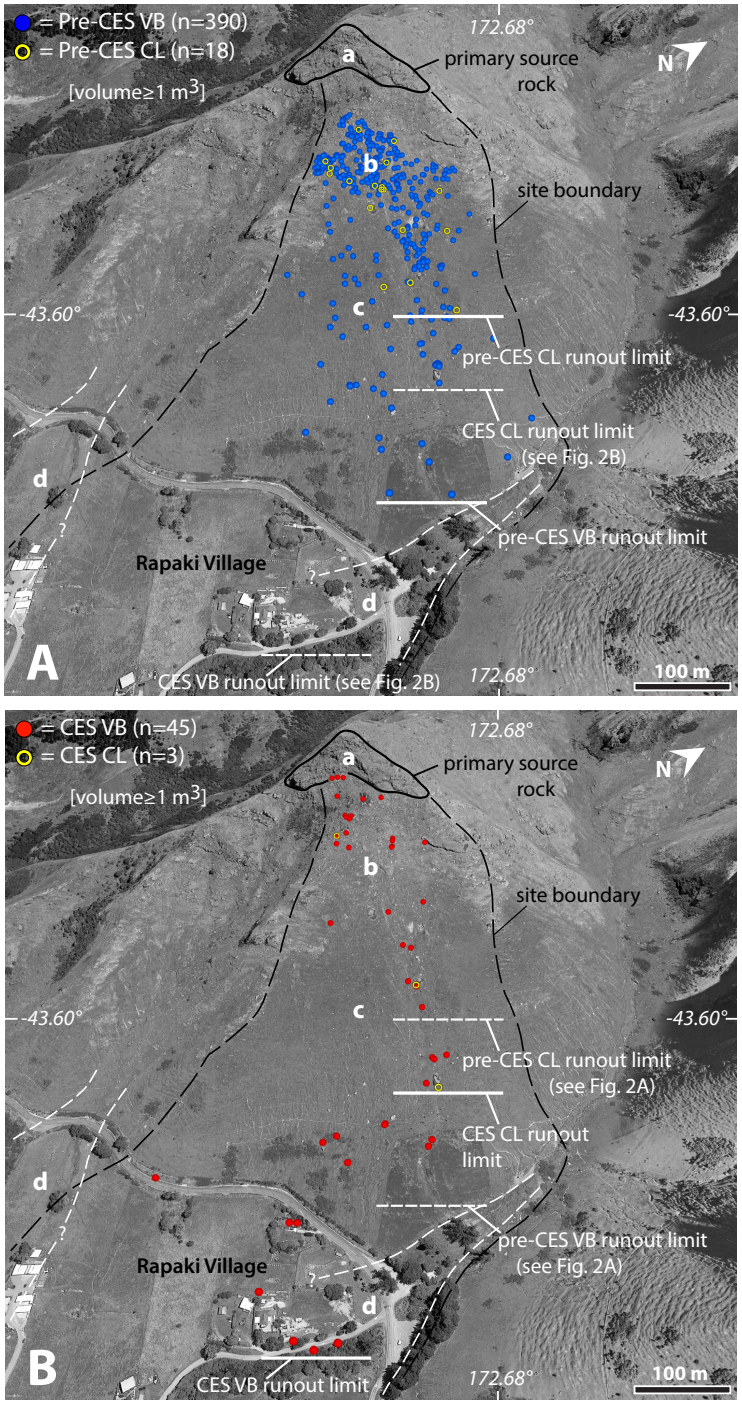

Figure 2

https://doi.org/10.5194/nhess-2019-178
Preprint. Discussion started: 11 June 2019

Natural Hazards and Earth System Sciences
Discussions

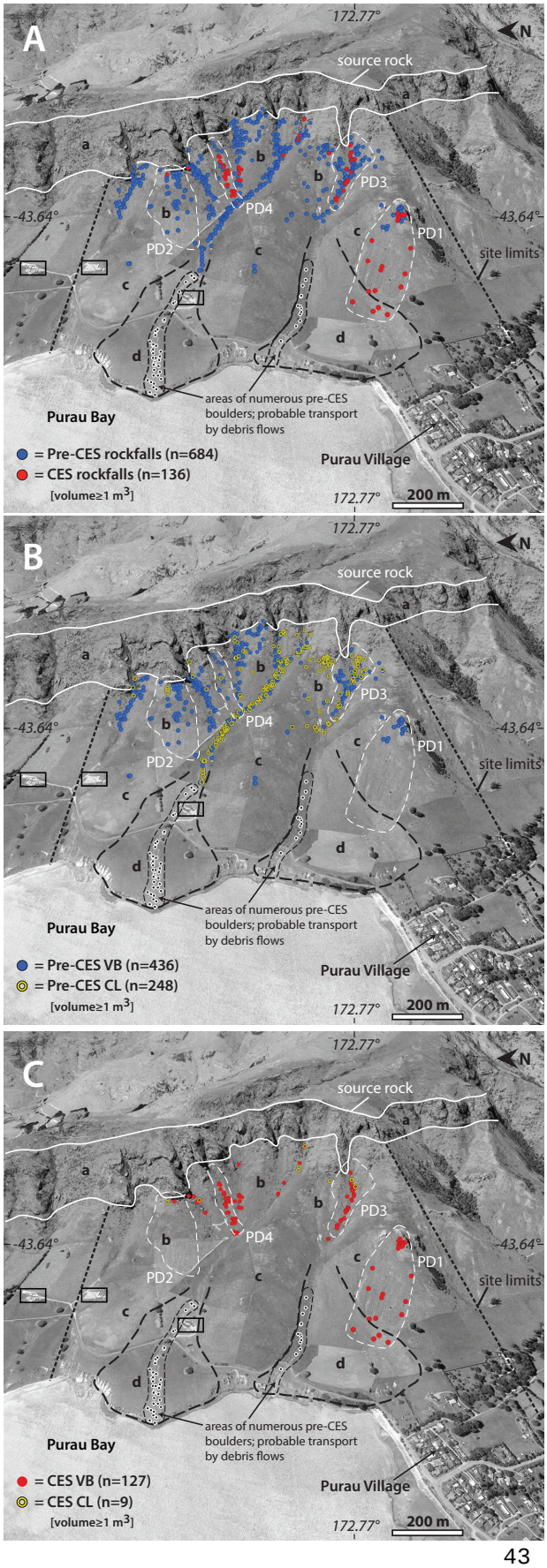

Figure 3

https://doi.org/10.5194/nhess-2019-178
Preprint. Discussion started: 11 June 2019

Natural Hazards and Earth System Sciences
Discussions

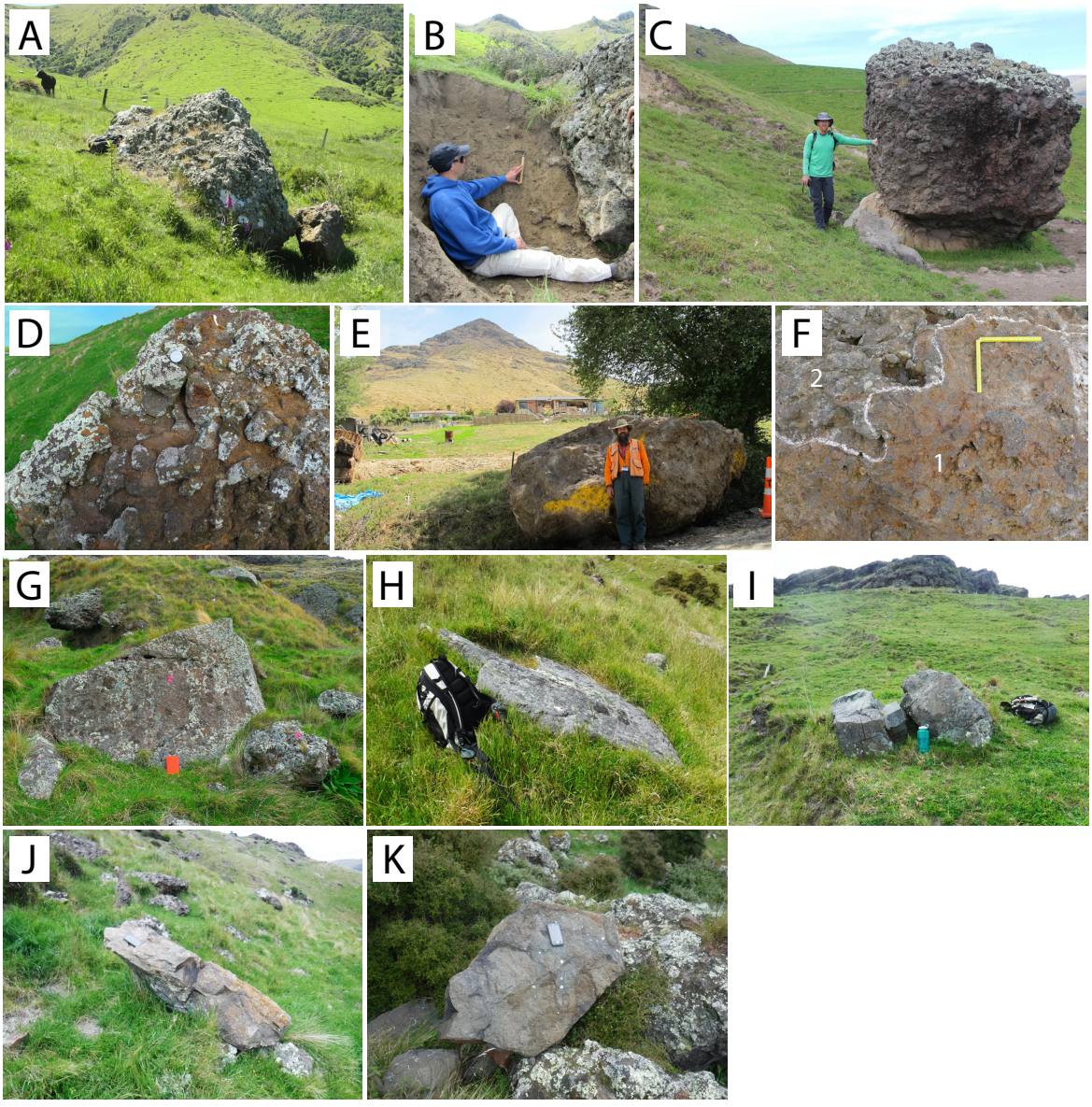

Figure 4

https://doi.org/10.5194/nhess-2019-178
Preprint. Discussion started: 11 June 2019

Natural Hazards and Earth System Sciences
Discussions
Open Access
EGU

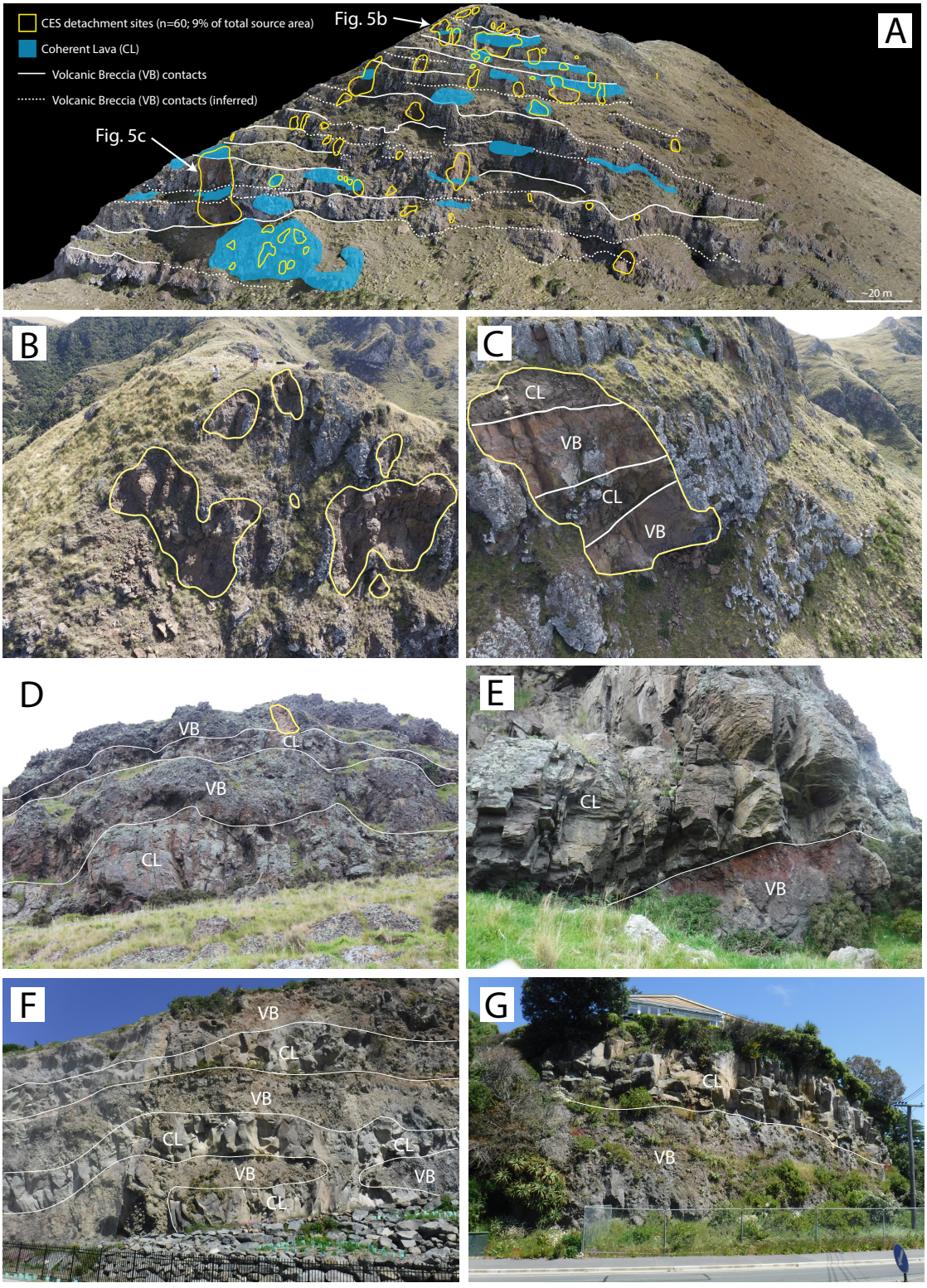

Figure 5

https://doi.org/10.5194/nhess-2019-178
Preprint. Discussion started: 11 June 2019

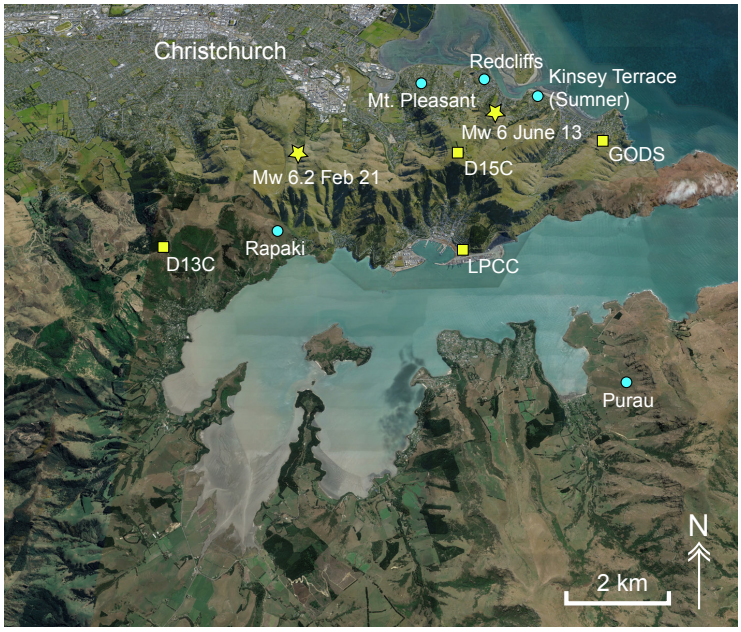

Natural Hazards and Earth System Sciences
Discussions
Open Access
EGU

Figure 6

https://doi.org/10.5194/nhess-2019-178
Preprint. Discussion started: 11 June 2019

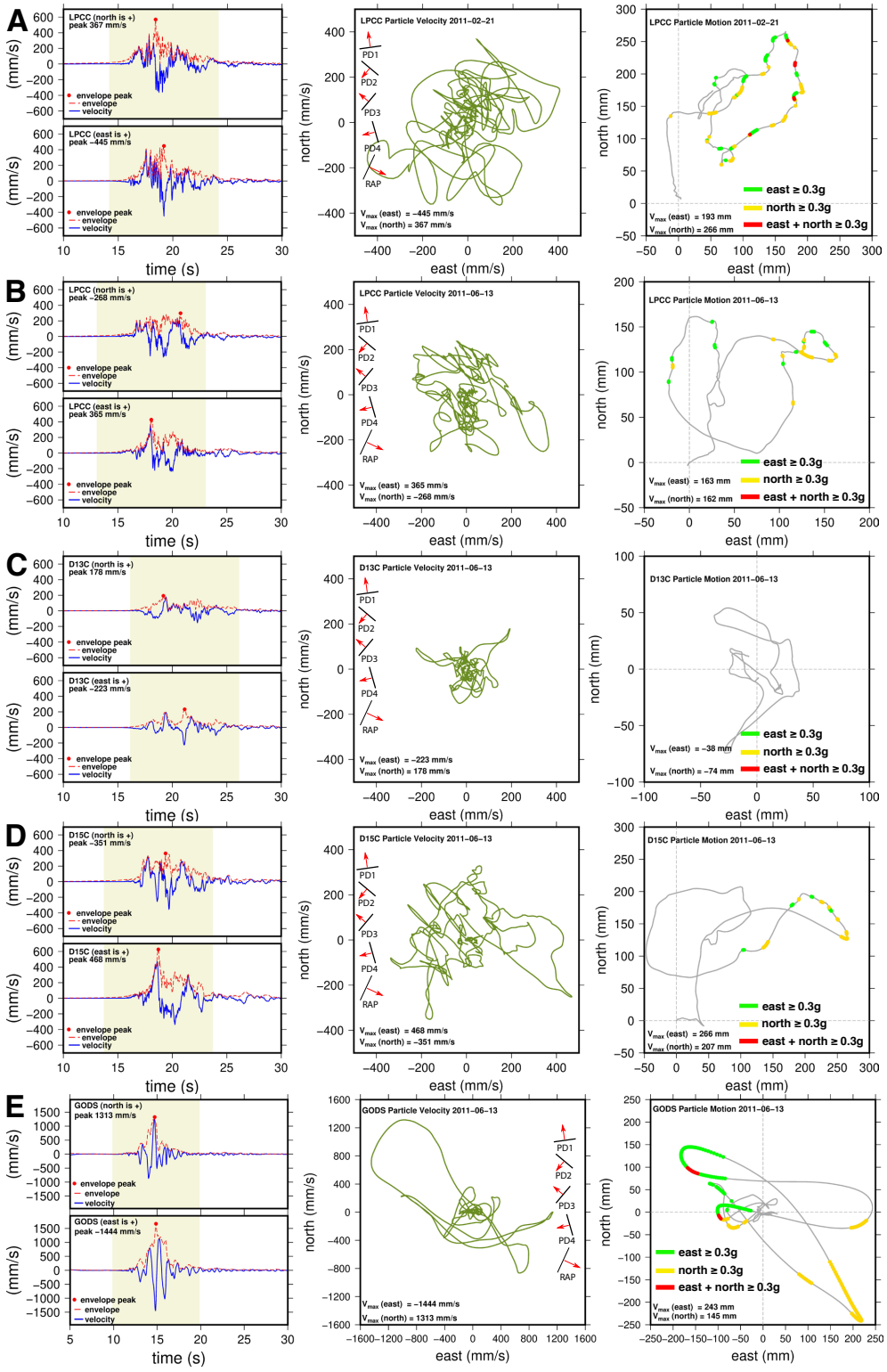

Figure 7

https://doi.org/10.5194/nhess-2019-178
Preprint. Discussion started: 11 June 2019

Natural Hazards and Earth System Sciences
Discussions
Open Access
EGU

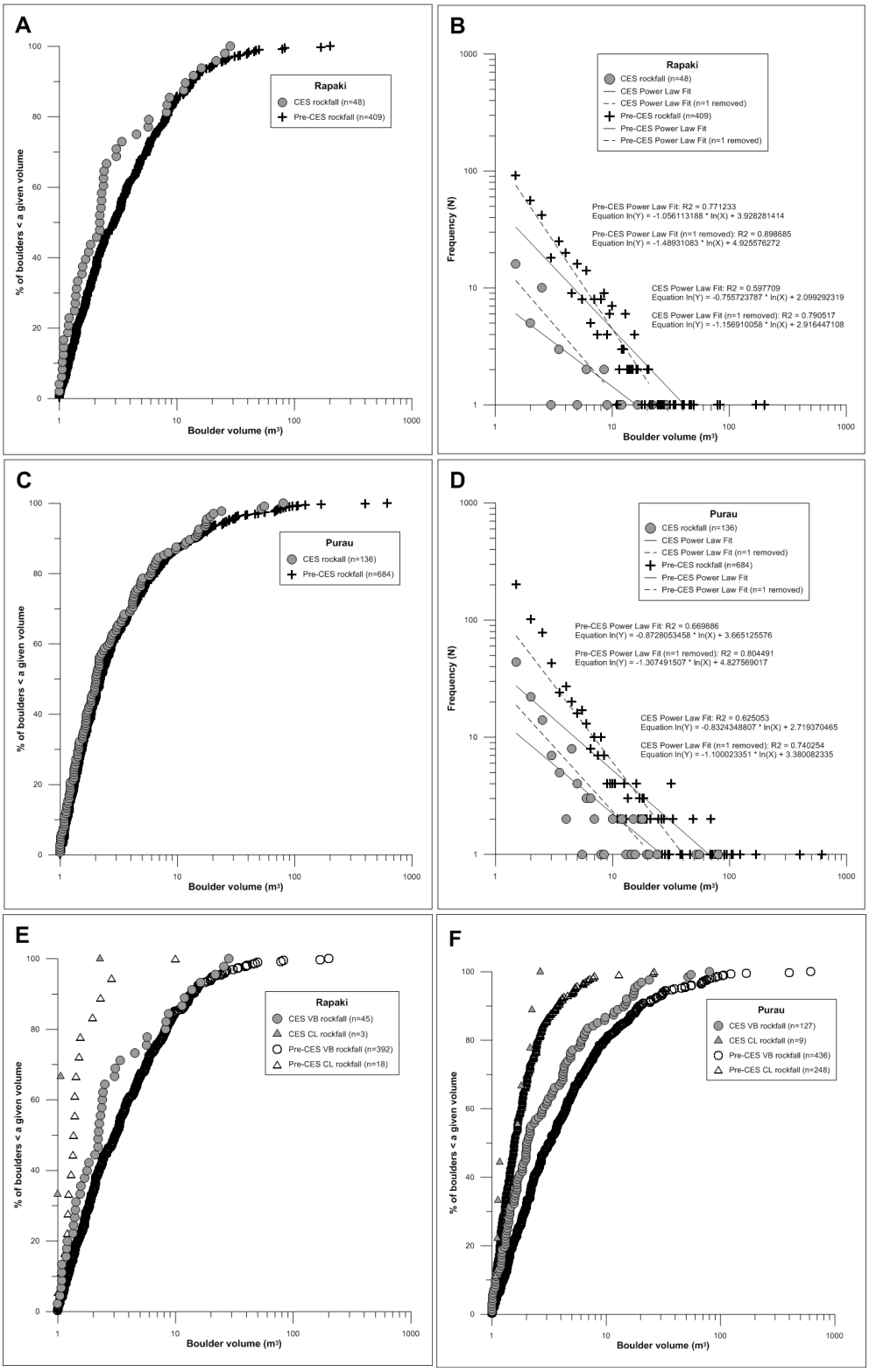

Figure 8

https://doi.org/10.5194/nhess-2019-178
Preprint. Discussion started: 11 June 2019

Natural Hazards and Earth System Sciences
Discussions
Open Access
EGU

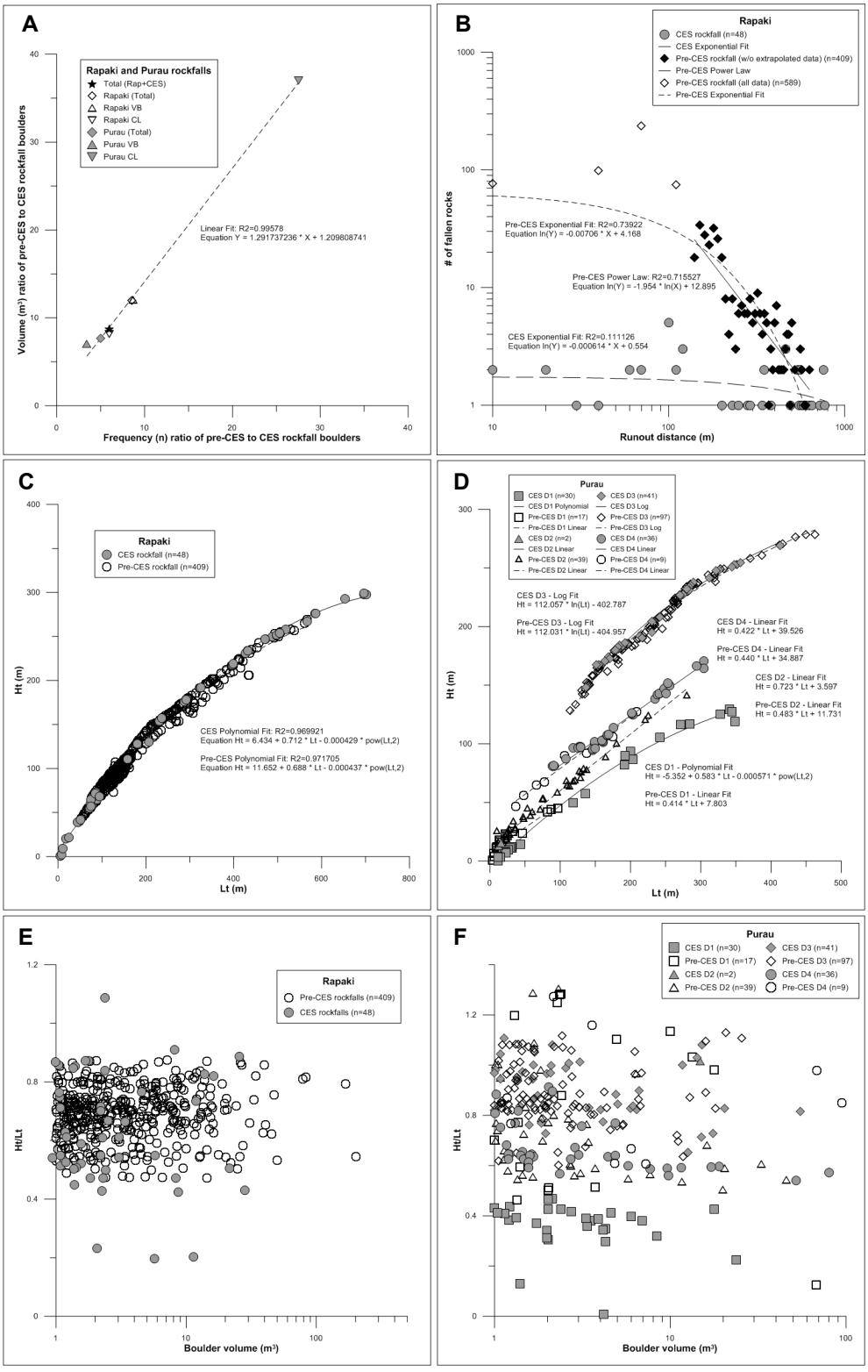

Figure 9

https://doi.org/10.5194/nhess-2019-178
Preprint. Discussion started: 11 June 2019

Natural Hazards and Earth System Sciences
Discussions
Open Access
EGU

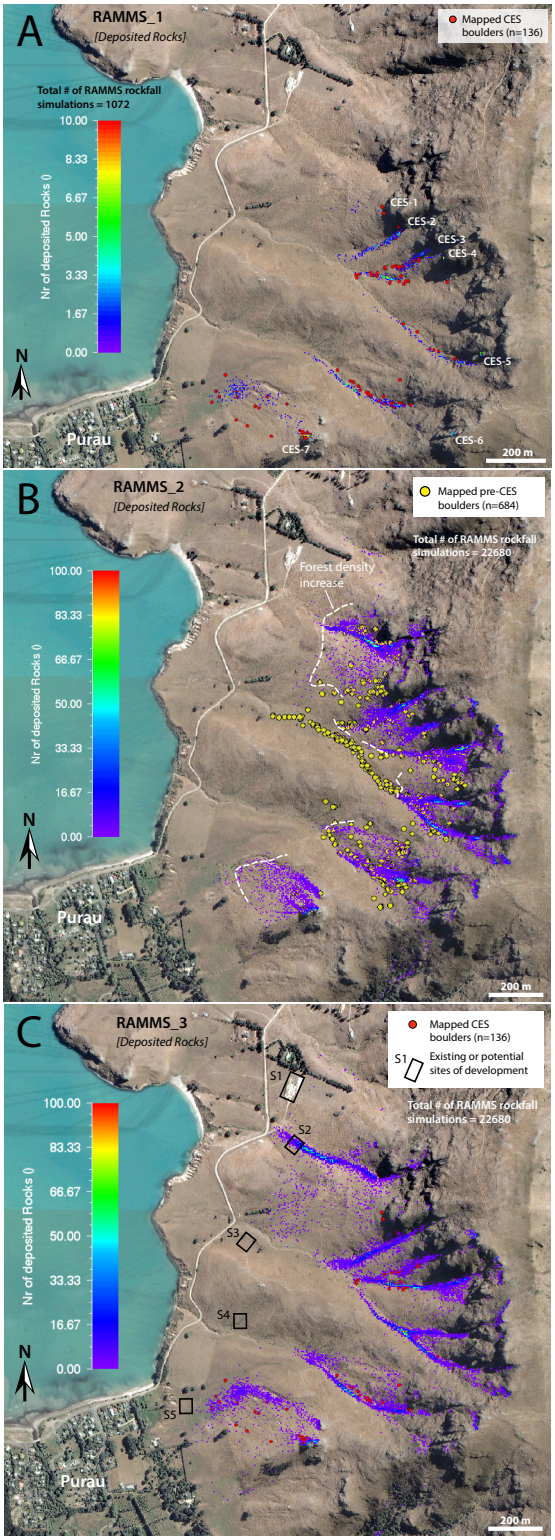

Figure 10

https://doi.org/10.5194/nhess-2019-178
Preprint. Discussion started: 11 June 2019

Natural Hazards and Earth System Sciences
Discussions

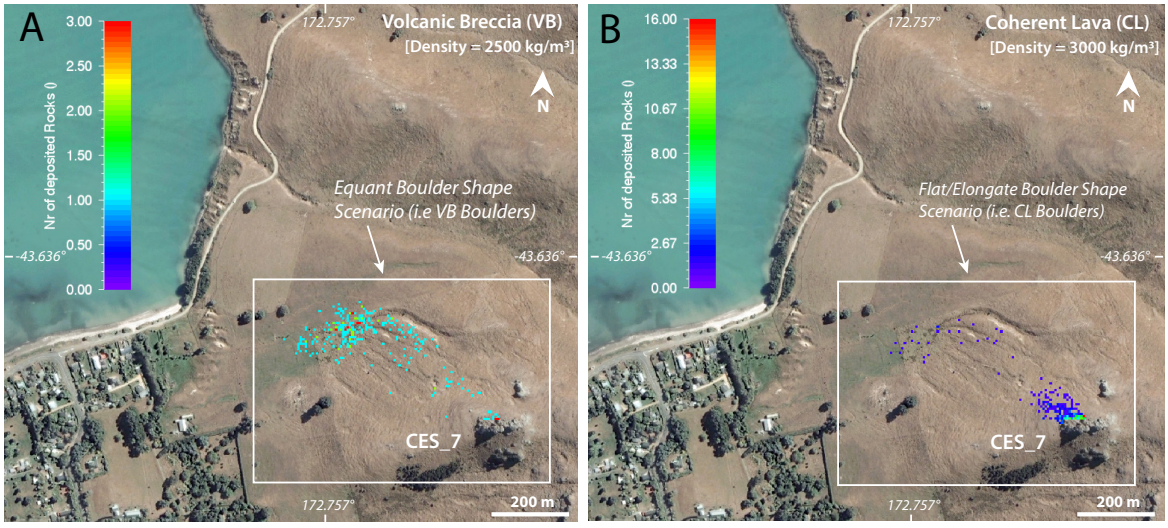

Figure 11

https://doi.org/10.5194/nhess-2019-178
Preprint. Discussion started: 11 June 2019

Natural Hazards and Earth System Sciences
Discussions
Open Access
EGU

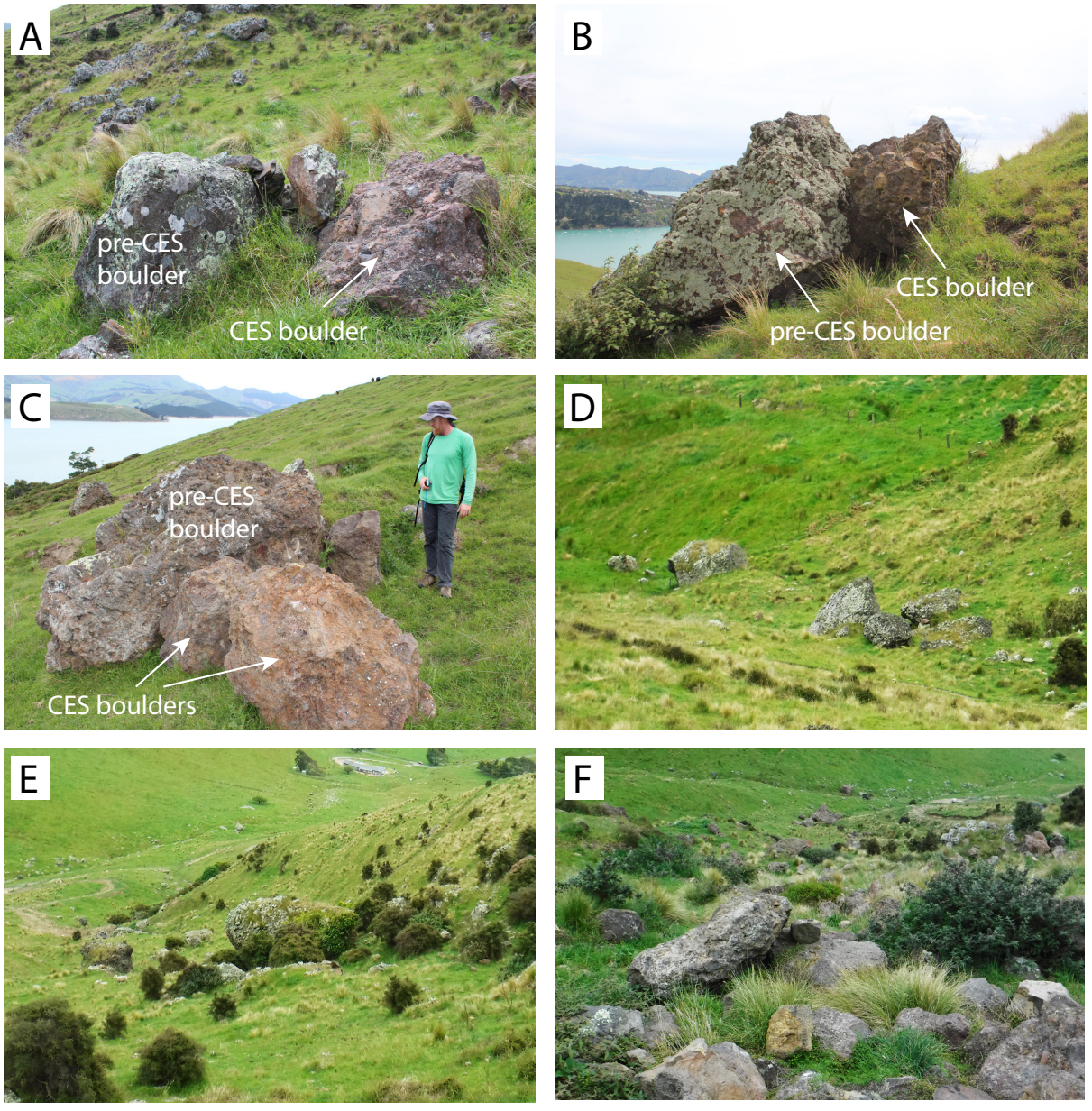

Figure 12

https://doi.org/10.5194/nhess-2019-178
Preprint. Discussion started: 11 June 2019

Natural Hazards and Earth System Sciences
Discussions

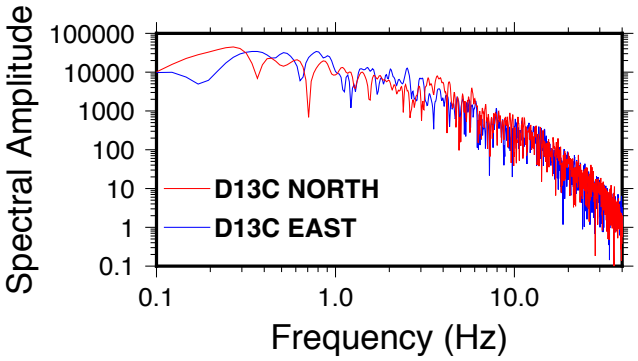

Figure 13

https://doi.org/10.5194/nhess-2019-178
Preprint. Discussion started: 11 June 2019

Natural Hazards and Earth System Sciences
Discussions
Open Access
EGU

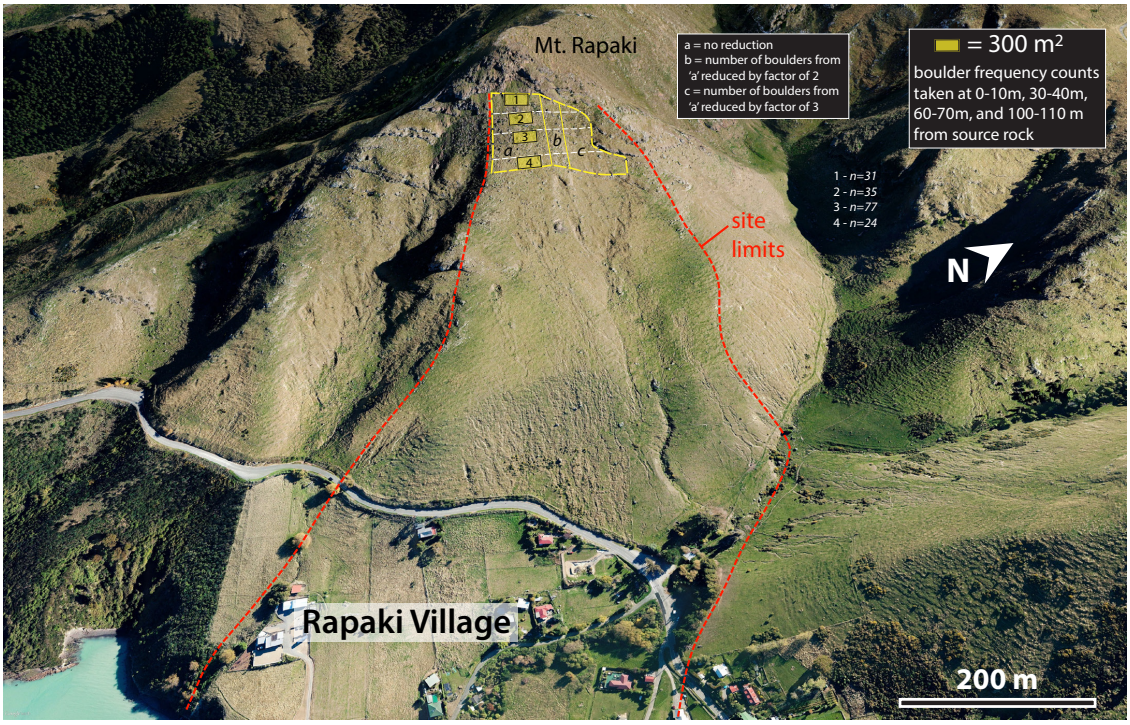

Appendix 1 - Figure A1

https://doi.org/10.5194/nhess-2019-178
Preprint. Discussion started: 11 June 2019

Natural Hazards and Earth System Sciences
Discussions
Open Access
EGU

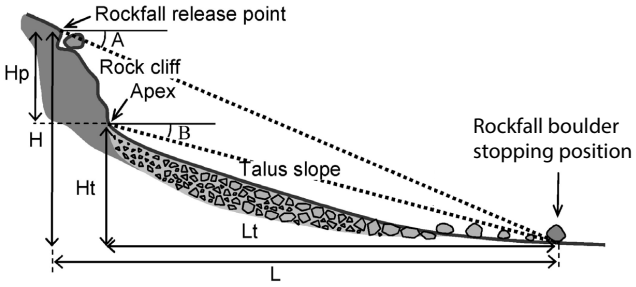

Appendix 1 - Figure A2

https://doi.org/10.5194/nhess-2019-178
Preprint. Discussion started: 11 June 2019

Natural Hazards and Earth System Sciences
Discussions

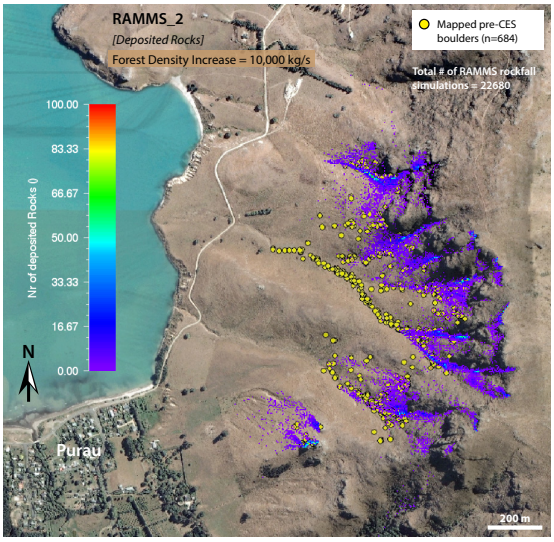

Appendix 1 - Figure A3

https://doi.org/10.5194/nhess-2019-178
Preprint. Discussion started: 11 June 2019

Natural Hazards and Earth System Sciences
Discussions

	μ_{min}	μ_{max}	ε	Drag layer coefficient	β	κ
Volcanic Rock	0.7	2.0	0	0.3	50	0.5
Loess and volcanic colluvium	0.45	2.0	0	0.5	30	0.6
Loess	0.3	2.0	0	0.5	30	0.5
Valley Terrain	0.2	2.0	0	0.9	25	0.5

Appendix 2_Table A1. Friction parameters chosen for each terrain type in RAMMS.

https://doi.org/10.5194/nhess-2019-178
Preprint. Discussion started: 11 June 2019

Natural Hazards and Earth System Sciences
Discussions
Open Access
EGU

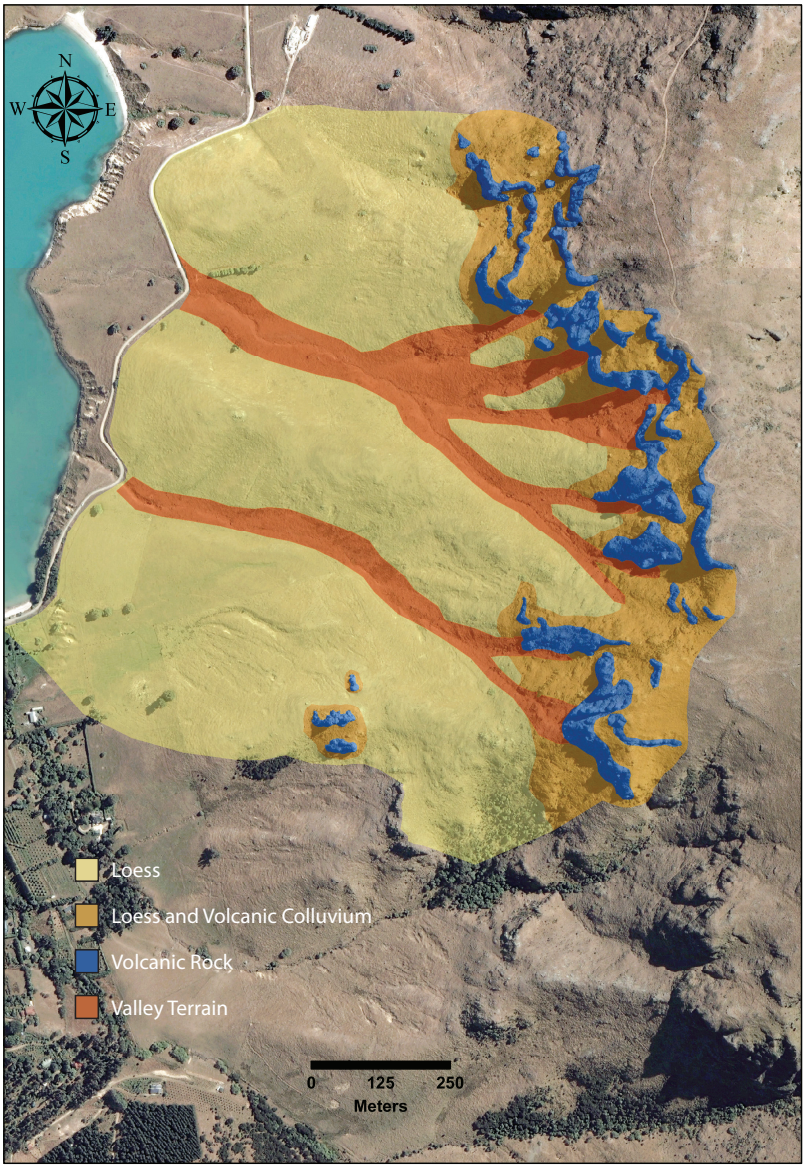

https://doi.org/10.5194/nhess-2019-178
Preprint. Discussion started: 11 June 2019

Natural Hazards and Earth System Sciences
Discussions
Open Access
EGU

https://doi.org/10.5194/nhess-2019-178
Preprint. Discussion started: 11 June 2019

Natural Hazards and Earth System Sciences
Discussions
Open Access
EGU

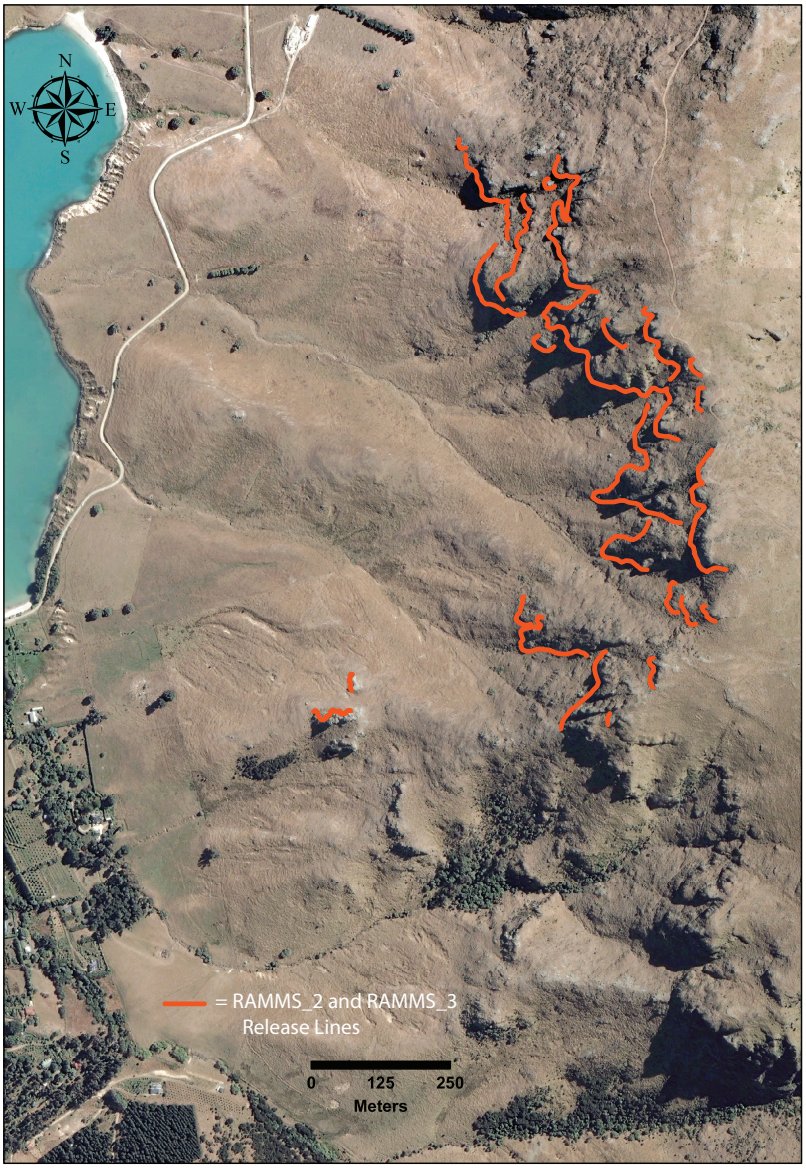

https://doi.org/10.5194/nhess-2019-178
Preprint. Discussion started: 11 June 2019

Natural Hazards and Earth System Sciences
Discussions
Open Access
EGU